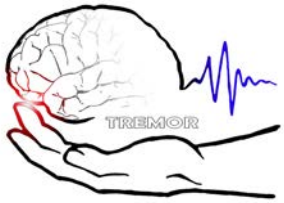

TREMOR. An ambulatory BCI-driven tremor suppression system based on functional electrical stimulation

Contract: FP7-ICT-2007-224051

Seventh Framework Programme, EU

Title:	D6.1 Strategies for FES active and semi-active tremor suppression
Author(s):	J.A. Gallego[1], A.D. Koutsou[1], E. Rocon[1], J.M. Belda-Lois[2], M. Castronovo[3], M. Goffredo[3], S. Conforto[3], T. D'Alessio[3], D. Popovic[4], L. Popovic[4], M.B. Popovic[5] and J.L. Pons[1]
Partner(s):	(1) CSIC, (2) IBV, (3) URT, (4) AAU and (5) UNA
Workpackage:	WP6
Date of preparation:	22.07.2011
Version number:	v4.0

Table of contents

Executive Summary

This document is a resubmission of deliverable D6.1 “Control strategies for FES active and semi-active tremor suppression,” prepared upon request of the reviewers in the Second Review Meeting.

The new version of the deliverable describes both control strategies for FES-based tremor suppression developed in the framework of the project. These strategies are the so-called active and semi-active strategies. The former is based on repetitive control theory, and aims at generating an oscillation that counteracts the tremor; therefore accurate tracking of tremor frequency and severity at every affected joint is mandatory. The latter relies on impedance modulation to filter out the tremor, leaving concomitant voluntary movement unaltered. We describe in this document the three versions (iterations) of both strategies that have been evaluated in patients; results on clinical and functional evaluation will be thoroughly presented in deliverable D8.2 “Case studies and analysis of functional, clinical and usability evidence of TREMOR system.”

Apart from the strategies themselves, the document starts with our simulation and experimental work on enhancement of stimulation selectivity by means of electrode arrays, although due to functional issues with the active garment (also reported in deliverable D8.2) the control strategies only consider conventional bipolar electrodes. When technological limitations with the active garment are circumvented, the controller can easily integrate matrix stimulation into its current implementation. Moreover, this deliverable also describes an easy-to-identify model of muscle response to FES. Finally, the document ends with a description of figures of merit employed to evaluate and compare tremor suppression strategies, and with an appendix where the protocol employed to interface with the TREMUNA stimulation is briefly reviewed.

Change history record

The overall organization of the manuscript has been kept with respect to the previous version (V3.0) submitted for review; section 1 introduces the deliverable whereas sections 2, 3, 4 and 5 correspond to the outcome of the activities of work packages WP6.1, WP6.2, WP6.3 and WP6.4 respectively. Section 6 in the original document has been included as an Appendix since it is basically related to a communication protocol (with the stimulators) and not to scientific research as the rest of the document. The information of sections 2 to 5 has been updated according to the Consortium activities; the organization has been thus revised in accordance, and in particular a more detailed review of the literature on each topic has been included.

As for section 2, we have included a novel model for FES-based tremor suppression together with its experimental evaluation (subsection 2.2). The remainder of the section is the same. Regarding sections 3 and 4, which deal with the so-called semi-active and active tremor suppression strategies, we have introduced the implementation and experimental evaluation of two new versions of both strategies (that are referred to as second and third version). The original content was included in epigraphs entitled first version of such strategy. The figures of merit of section 5 have also been updated based on our recent results; the development of our new method is summarized.

Introduction

Pathological tremor is a major cause of disability; as a matter of fact 65 % of people with upper limb tremor reports serious difficulties when performing their activities of daily living [1]. Moreover, one out of four patients does not benefit from any of the existing therapy. Under such circumstances, the research community has devoted considerable effort to develop alternative systems to manage upper limb tremors.

The approach that has received more attention is the application of biomechanical loads on the affected limb. The effect of external forces (elastic or viscous for example) and masses on physiological tremor were already thoroughly described in 1974 [2]. Alteration of the properties of pathological tremors was also early pointed out, e.g. [3], see [4] for a more detailed review. As a consequence, a series of works demonstrating that increased inertia and/or damping could lead to a reduction of tremulous movement appeared [5, 6], giving rise to the possibility of orthotic management of tremors based on biomechanical loading [7].

The systems to compensate for tremors exploiting this principle –and in general any rehabilitation device– can be classified into two categories: i) ambulatory wearable orthoses, and ii) non-ambulatory table or wheelchair mounted devices. While the latter have already given rise to commercial products like the Neater Eater [8], the MIT dampened joystick [9], the Controlled Energy Dissipation Orthosis [10] or the Modulated Energy Dissipation Arm (cited in [7]), the former are still a matter of research.

Among the wearable robotic systems, the WOTAS exoskeleton constitutes the most relevant attempt [11]. This exoskeleton, developed by some partners of TREMOR, applied biomechanical loads between upper limb segments to attenuate the tremor. WOTAS implemented two control strategies: i) a viscous loading of the affected joint, and ii) notch filtering at tremor frequency [11], which serve as the basis for what in TREMOR are referred to as semi-active and active strategies. Evaluation in a group of 10 tremor patients suffering from different disorders showed a consistent reduction of 40 % in tremor severity, attaining up to an 80 % in the most severe cases. The major limitations of the system were the difficulty to transmit the load through soft tissues, which was more evident in those with moderate tremor, and the aesthetic and usability issues the users reported.

Application of biomechanical loads through direct activation of upper limb muscles emerges as a way to circumvent these two problems. Moreover, preliminary evidences on the feasibility of such approach were already reported in Prochazka's seminal work [12, 13]. As a matter of fact, two other research groups are working on similar approaches. One of them uses a concept similar to our semi-active strategy [14], while the other employs a controller that resembles to our active strategy [15]. This was the approach followed by Prochazka and colleagues too [12].

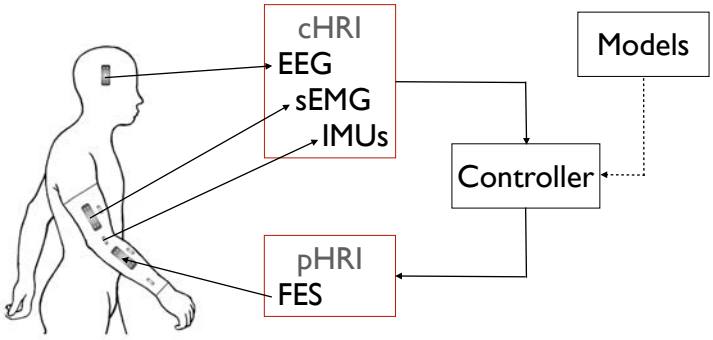

Figure 1. Scheme that represents the control architecture implemented in the TREMOR wearable robot.

This deliverable presents the concept and implementation of the physical Human-Robot Interface (pHRI) of the TREMOR wearable robot. Such interface is in charge of selectively applying biomechanical loads through functional electrical stimulation (FES) in order to attenuate the tremor, and minimally interfering on the concomitant voluntary movement. The controller that drives the pHRI considers tremor parameters as derived from the cognitive Human-Robot Interface (cHRI). Tremor features, i.e. tremor onset, amplitude and frequency, are extracted at every targeted degree of freedom, namely wrist flexion/extension and elbow flexion/extension. A scheme depicting the overall architecture of the controller is shown in Fig. 1. The figure represents how the information derived from the different sensors modalities that constitute the multimodal BCI that implements the cHRI are fed into the controller. The controller then generates stimulation commands based on this input and on the conclusions drawn from the simulation work carried out in the framework of work package WP5. Details about the BNCI are given in deliverable D4.1 "BCI algorithms for tremor identification, characterization and tracking;"

our work on simulation of tremor and FES-based strategies is described in deliverables D5.1 “Musculo-skeletal model optimized for a real-time semi-active and active control in a simulation environment” and D5.2 “Musculo-skeletal model optimized to provide the appropriate stimulation patterns to attain a desired biomechanical characteristics or motion/force desired at joints.”

Independent joint control is implemented since tremor is a local phenomenon, and can migrate proximally when the attenuation starts [16]. Moreover, it enhances system’s modularity and ease of exploitation.

This deliverable describes the work carried out in work package WP6 “Control strategies for FES based active and semi-active tremor suppression.” This work package was coordinated by CSIC, who led the various tasks. The objectives of this work package were:

- To link the information provided by the multimodal BCI (WP4) and the inverse dynamic musculoskeletal model (WP5) in a semi-active and active tremor suppression strategies.
- To develop an impedance control approach for the semi-active tremor suppression strategy.
- To develop a model based controller for the active tremor suppression strategy.

The following tasks were defined in order to meet these objectives:

1. *Development of a model for selective FES muscle stimulation*. This task aimed at merging the information provided by the different sensors modalities and the inverse dynamic musculoskeletal model in a finite element model to provide insights into the mechanisms that make it possible to attain greater muscle selectivity by selection of the adequate stimulation patterns.
2. *Development of a control approach for semi-active tremor suppression*. This task aimed at developing a control law to drive an anatomical joint to specified apparent inertia, damping and viscosity as a means of compensating for the tremor.
3. *Development of a control approach for active tremor suppression*. This task was devoted to the development of a control strategy that applies an out of phase and opposing force to the targeting joint.
4. *Definition of figures of merit*. This task aimed at proposing a series of metrics to compare the performance of the different active and semi-active tremor suppression strategies, complementing the clinical and usability measures proposed in work packages WP1 and WP8.
5. *Definition of strategies for rule-based control of the multi-channel FES hardware*. This task aimed to developing a control framework for real-time interaction with the novel FES system developed in the framework of work package WP3.

This document is organized as follows. First we present our simulation and experimental study on selective muscle activation with array electrodes, therefore addressing objective 1. Next we present an easy-to-identify joint model that was developed as a plant to be exploited by the controllers. The next sections describe the semi-active and active tremor suppression strategies, which constitute objectives 2 and 3. The theoretical description is accompanied by representative examples. As for the active tremor suppression strategy, we have also developed a version that relies only on surface EMG as sensory input, while the others exploit joint kinematics as recorded by inertial sensors. The document ends with a description of the figures of merit employed to evaluate tremor. Therefore, this section addresses objective 4. Finally, in the appendix we summarize the communication protocol used to control the TREMUNA stimulators, and hence to implement the control strategies, which is related to objective 5.

1. Development of a model for selective FES muscle stimulation

This section summarizes work on task WP6.1 "Development of a model for selective FES muscle stimulation." This task aims at developing a method to enhance selectivity when artificially activating the upper limb muscles with FES. To do so, a simulation study and an experimental protocol have been developed. Selectivity enhancement aims not only at improving the quality of the movement elicited, but also at fatigue minimization and optimization of comfort.

URT led this task and collaborated with CSIC and IBV in the different activities. A number of research visits and telemeeting were held to coordinate the work. The final outcome consisted in a series of computational models and experimental methods. Details on the work plan followed are given next:

- Development of a computational model that simulates stimulation by conventional FES electrodes in two steps.
- Validation of this model by comparing its predictions with recordings from a control group in the same conditions.
- Extension of the computational model to account for electrode array stimulation (reproducing the properties of the active garment).
- Validation of this second version of the model, i.e. to assess the performance of the model when an array electrode is implemented.
- Motivated by the literature and model results, we developed a protocol for selection of optimal pads. Optimal pads are those that elicit more clearly the targeted movement.
- Validation of the selectivity protocol in control subjects.

In parallel, we have worked on a model that relates stimulation parameters to joint kinematics. Such model also estimates joint impedance (modelled as a second order process). The model is identified in each muscle group for every patient, and is intended to serve as plant for future model based strategies. Work on this topic has followed the following work plan:

- Development of the single joint model.
- Validation on control subjects in static conditions.
- Preliminary validation on tremor patients, also in static conditions.

1.1. Development of a finite element model of muscle selectivity

The scientific literature has shown that array electrodes provide improved efficacy and selectivity when compared to traditional electrodes given that adequate electrode design (number and geometry of individual electrodes, material) and stimulation parameters (amplitude, frequency and pulse duration) are chosen. It must be highlighted though, that the underlying physiological principles that render this possible have not been fully elucidated yet. On the other hand, array electrodes may also circumvent misplacement problems (of the electrodes with respect to the muscles that elicit the targeted movement) by employing an automatic method for intelligent selection of electrode geometry and stimulation parameters. A similar procedure can also be envisioned to optimize the stimulation in different limb poses, e.g. for the forearm muscles.

Traditionally, the mechanisms that underlie fibre recruitment under neurostimulation have been investigated with mathematical models [17, 18]. The departure point is that perturbation of the transmembrane potential of an axon can initiate nerve excitation, i.e. generate an action potential. In their seminal work Hodgkin and Huxley [19] developed and experimentally validated the first mathematical model that describes the transmembrane potential based on the intracellular and extracellular ionic concentrations. This work formed the basis for a large number of works presenting various refined axon excitation models for different types of axon excitation or inhibition [17, 20-22].

Later, McNeal embedded such an axon model in a purely resistive volume conductor that described the surrounding potential distribution [17], developing the first combined model referred to as two-step model. The first step describes the electrical potential distribution within the electrode-tissue interfaces and the bulk tissues (volume conductor) based on the exciting electrodes. The second step describes the complex behaviour of the axons' transmembrane potentials, which depends upon the spatiotemporal potential distribution along the axon. This two-step approach is implemented in most FES models [17, 23-28] and is applied to peripheral and central nerves, for anodic and cathodic currents.

The majority of two-steps models found in literature apply currents via couples of electrodes [22, 23] and mainly focus their attention on the model behaviour with respect to the stimulation parameters, rather than to the

electrodes design. One of the first studies on the effects of electrodes' shape on nerve excitability, has been conducted by Kuhn et al [29]. In this study the authors used their FES model [28] to analyse nerve behaviour with different electrodes configuration and gel resistivities. It has been found that the resistivity of the electrode–skin interface layer should be adapted depending on the size of the gaps between the array elements.

On the basis of this, this epigraph presents our two-step finite element model that simulates activation of motor neurons by transcutaneous neurostimulation. The model, which has adequate spatial resolution (in voxels) to account for the anatomical properties of the arm, calculates the electrical field produced in the tissues by any arbitrary distribution of electrodes placed on the arm surface. The electrical characteristics of both the different tissues and the electrodes are carefully represented. We simulate both (traditional) bipolar electrodes and the array implemented in the active garment to gain insight into their performance. The former has never been addressed in the literature.

Therefore, the objective of this task is twofold: on the one hand it is devoted to unravelling the mechanisms that render matrix stimulation more effective than bipolar stimulation, on the other hand it is focused on the development of an experimental protocol to identify for each patient the optimal electrode shape (i.e. which electrodes in the array to be activated).

1.1.1. Model overview

We have developed a two-step model that includes the passive properties of tissues and the active characteristics of the nervous system (Fig. 2).

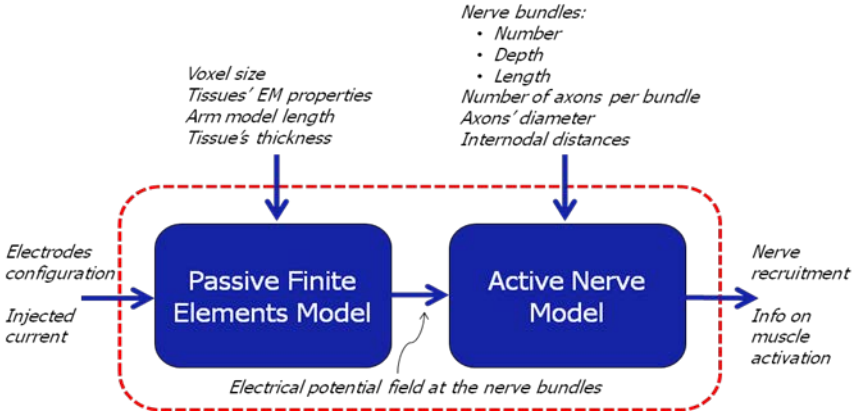

Figure 2. Overview of the muscle model developed.

The human tissues are included in the passive part of the model, the first step. The muscle is represented by a transient quasi-static finite element (FE) model involving a simplified cylindrical multi-layered structure, where the human muscles (i.e. skin, fat, bone cortical, bone marrow and muscle) are characterized by their conductive and dielectric properties.

The introduction of the relative electric permittivity constants (Table I) allows including also the capacitive effects arising in the layers, typically neglected in the low frequency range associated to FES signals. The 20 cm long cylinder contains skin, fat, muscle and bone layers with thicknesses of 1.5 mm (skin), 6 mm (fat), 24 mm (muscle), 5.5 mm (cortical bone) and 5.5 mm (bone marrow).

The equations of the FE model are solved by a finite integration time-domain solver (CST EM Studio®), which computes the electrical field produced into the tissues by the current injected through the electrodes placed on the arm surface.

The resistive and capacitive electrical properties of each tissue have been taken from literature [30] and are shown in Table I. The model has spatial resolution of 1 mm^3/voxel, in accordance with anatomical studies.

	Skin	Fat	Muscle	Bone
Conductivity (S/m)	0.0014	0.03	0.35	0.02
Permittivity (F/m)	6000	25000	120000	3000

Table I. Electrical properties of tissues.

In a second step, the results from the FE model (the so-called passive model) are fed to the active part of the model, which determines the effects of the effect of the injected current on the motor neurones. The active model

thus represents the dynamic properties of the nervous system. It is inspired by the axon structure in [22] and has been developed in the NEURON simulation environment. The model calculates whether each axon is active or not.

The model consists in a complete representation of the myelinated nerve, where both myelin passive properties, axon properties at resting phase and K^+, Na^+ and leakage currents at the nodes of Ranvier are included. Axons are grouped in nerve bundles buried at different depths from 0.6 to 1.5 cm with 0.1 cm spacing. Each bundle is composed of 100 axons whose typology and diameter are distributed as in Fig. 3, according to the literature [31]. Distances between consecutive nodes of Ranvier ranges from 0.4 to 1.6 mm.

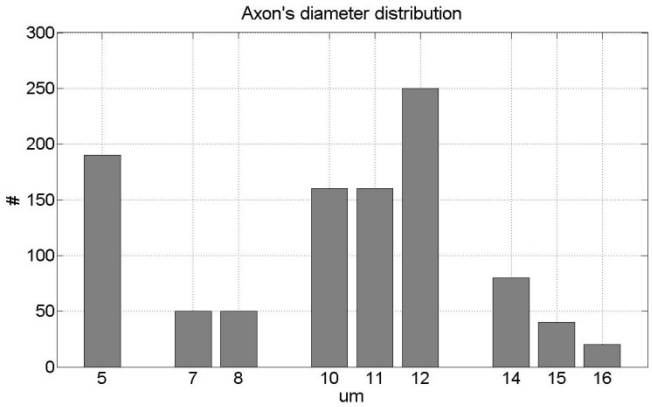

Figure 3. Histogram representing the distribution of diameter of 1000 axons. The abscissa represents the axon diameter in μm, the ordinate the number of axons.

The link between the passive and the active model is established by assigning the current values, as computed via the passive model, to the corresponding injected currents at the nodes of Ranvier in the active model. Therefore, the proposed active model takes account of the time-varying currents corresponding to each node of Ranvier and gives membrane potentials for each axon.

The output of the proposed arm model is the number of active axons, i.e. nerve recruitment. Muscle contraction is considered to occur if nerve recruitment is over 10%.

It must be noticed here that this model is not intended to be personalized for every patient, but is aimed at comparing the effect of different electrode configurations, the optimal stimulation waveform and current amplitude values, and to understanding the summation effects of multiple electrodes and the possibility of applying different time sequences for pulses.

1.1.2. Validation of the model

We validated the model by comparing its output with the experimental results extracted from a control group.

The protocol employed was as follows. Regarding the simulation, two Ag/AgCl electrodes of 1.5 cm diameter (inter-electrode distance of 2 cm) were virtually applied on the surface of the cylindrical structure. Square wave pulses with pulse amplitude between 0 mA and 25 mA (steps of 1 mA) and duration between 100 μs and 1000 μs (steps of 50 μs) were used as stimuli. Repetition frequency was set at 20Hz. These stimulation parameters were used to run the overall model, extracting the electrical field produced in the tissues by the electrodes, and the nerve behaviour. As for the experimental tests, 6 healthy subjects (aged 20-26 years, 3 male, 3 female) with no clinical or neurophysiological disorders were recruited. All subjects gave informed consent. The median nerve was stimulated at the biceps brachii level by using two adhesive Ag/AgCl electrodes of 1.5 cm diameter connected to the electrical stimulator Micromed® Energy Twin. A Compex® motor point pen was used to accurately locate the motor point: it was moved over the upper arm to find the point that required the least amount of current to generate biceps brachii contraction. Therefore, the cathode and anode were placed in the middle of the upper arm and on the motor point respectively. The same square wave pulses used in simulation were applied: pulse amplitude between 0 mA and 25 mA (steps of 1 mA) and duration between 100 μs and 1000 μs (steps of 50 μs), and frequency set at 20Hz.

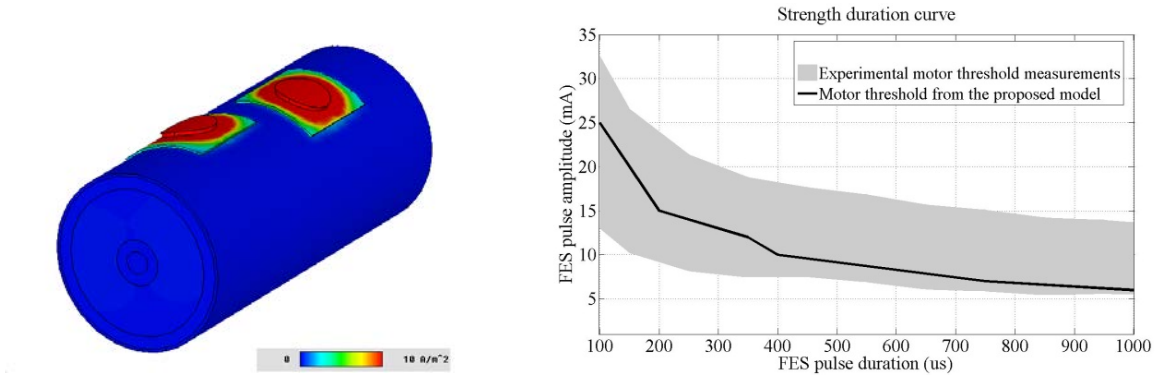

(a) (b)

Figure 4. Comparative results with a pair of electrodes. (a) Current distribution obtained with the model. (b) Strength duration curve derived from the model (solid black line) overimposed on the experimental motor threshold (grey surface).

Muscle behaviours were compared in terms of motor thresholds, i.e. strength duration curve (SDC) defined as the relationship between pulse durations and amplitudes corresponding to muscle contraction. Fig. 4(a) shows an example of the time-varying current density distribution across the whole structure that has been numerically computed by the solver; Fig. 4(b) compares the SDC range from experimental tests with the SDC obtained with the proposed arm model.

The SDC trend is consistent with the results reported in literature [30]. Moreover, the motor thresholds obtained from the proposed arm model are in the range of the experimental ones for the subjects who participated to the study. These results provide an experimental validation of the model when bipolar configuration is employed.

1.1.3. Simulation of array electrodes

This section presents two simulation studies addressing stimulation with an array of 2x2 conventional electrodes and a realistic representation of the sewn electrode array implemented in the active garment.

First simulation tests were conducted with 4 Ag/AgCl electrodes of 1.5 cm diameter placed as a 2x2 array with inter-electrode distance of 0.5 cm. A reference electrode was placed 2 cm from the array and pulses of 5 mA, 400 μs and 20 Hz were used. Different configurations of active electrodes were considered.

Fig. 5 compares nerve recruitment obtained with a pair of electrodes at 15 mA, the 2x2 array with 2 electrodes at 5 mA and the whole array with 3 electrodes at 5 mA. The outcome of the stimulation is defined as the number of active axons with respect to their diameters.

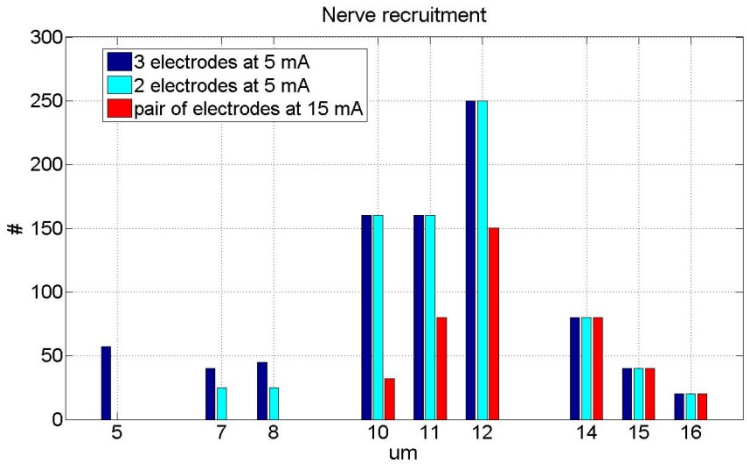

Figure 5. Nerve recruitment measured as number of active axons (with respect to their diameters) obtained for different electrode configurations, when simulating an array of 2x2 conventional electrodes.

Our results suggest that array electrodes induce nerve behaviour which is comparable to that obtained with one pair of electrodes. Bipolar electrodes however, are fed by a pulse producing higher current density distribution. Since discomfort and pain could be reduced by decreasing current density in tissues [32], this comparative study gives simulation evidences to the maximization of comfort when using array electrodes.

As mentioned above, the second study aimed at simulating arm behaviour with the sewn electrode array designed in TREMOR. To this aim, a 5x5 matrix of Ag/AgCl electrodes (1 cm diameter; 0.5 cm inter-electrode distance) was been applied on the cylinder (skin) surface; a 2x2 cm^2 reference electrode was placed 5 cm from the array, Fig. 6.

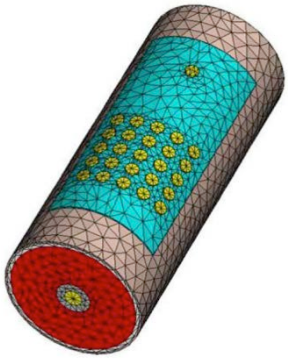

Figure 6. Appearance of the FE model of the arm with the TREMOR array electrode on it.

In the first phase of this study, two different electrodes were separately fed by square wave with the following characteristics: current amplitude 5 mA, pulse duration 300 μs and stimulation frequency 30 Hz. The electromagnetic field into the cylindrical structure was solved and compared with the one obtained by feeding the two electrodes at the same time and with the same stimulation wave. Fig. 7 shows an example of the time-varying current density across the structure at 20 mm depth. Our results suggest that the superposition principle can be applied to the proposed passive model, i.e. the current at a given place and time obtained in response to two or more electrical stimuli is the sum of the responses that would have been caused by each stimulus individually.

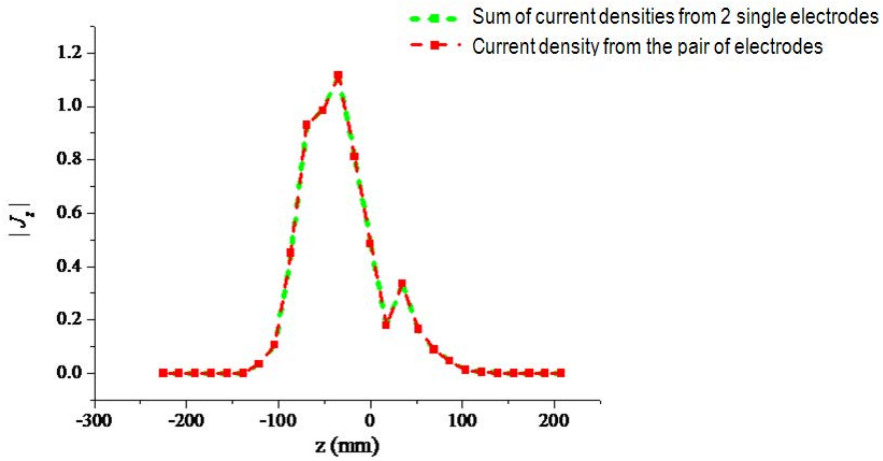

Figure 7. Example of the superposition principle applied to current densities in the model: the sum of the current densities obtained by feeding two electrodes separately (green line) is compared to the current density obtained by feeding them with the same stimulation wave at the same time (red line). The abscissa represents the cylinder longitudinal axis.

A second round of simulation tests was carried out. This protocol considered four patterns of 8 active electrodes in the 5x5 array, as shown in Fig 8(b). Square wave pulses with the following characteristics current amplitude ranging form 1 to 5 mA (the same value was applied to each electrode), pulse duration 300 μs and stimulation frequency 30 Hz were applied to each active electrode.

Fig. 8(a) shows the results in terms of nerve recruitment (percentage of active axons): pattern D presents the highest nerve recruitment curve, i.e. lower pulse amplitudes on every electrode (threshold at 1.7 mA) are sufficient to generate muscle contraction (defined as nerve recruitment higher than 10%, see above). Conversely, patterns A, B and C show lower recruitment with thresholds at 2.5 mA and 3 mA respectively. In particular, patterns A and B present completely overlapped curves because of the symmetric nature of both the model and the patterns.

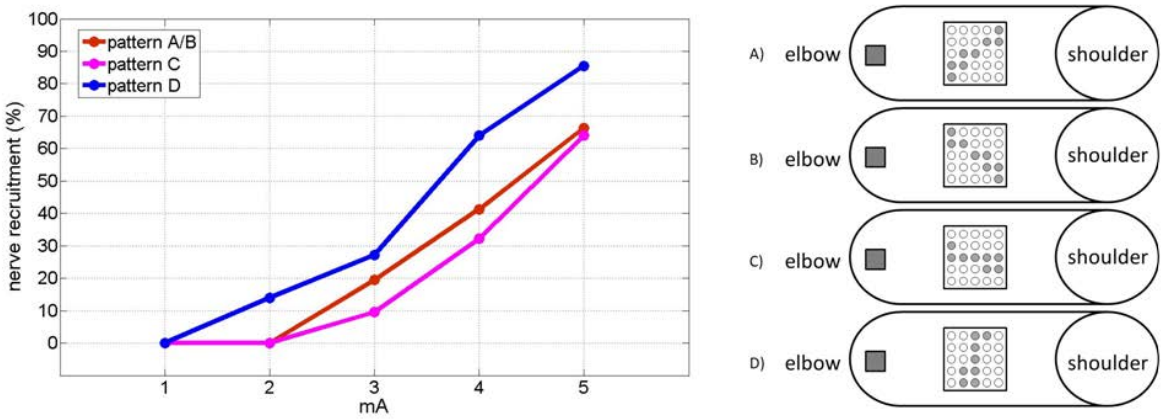

(a) (b)

Figure 8. Assessment of nerve recruitment when activating 8 electrodes of the TREMOR array electrode : (a) nerve recruitment (defined as percentage of active axons) vs. stimulation amplitude, (b) representation of the active electrodes for each of the four patterns.

This result suggests that spatial distribution of active electrodes in the array is a critical factor when eliciting a muscle contraction. Moreover, our simulations indicate that the more widely distributed (with respect to the reference electrode) the electrodes, the lower the current amplitude needed to contract muscle. Unfortunately this study could not be replicated in patients, since for the biceps brachii the stimulation amplitudes over 1 mA induced very painful sensations in most of the subjects recruited for the study.

Nevertheless, an important result of this study is that a smart selectivity algorithm, which prefers widely distributed active electrodes can optimise the trade-off between FES efficiency and subject's comfort. An experimental means of obtaining these optimal electrode configuration is given below.

1.1.4. Selectivity algorithm

We decided to use transcutaneous (surface) electrodes in TREMOR because of their reduced invasiveness and enhanced comfort, but at the cost of the reduced stimulation accuracy that can be attained. Reduced selectivity is motivated by the fact that it is impossible to know precisely the sensory-motor pathways that the electrical charge inserted will follow [33], since it depends on the current distribution in skin, fat and muscle, which in turn is governed by their electrical properties [34] and those are very hard to estimate.

As mentioned above, it has been established, nevertheless, that the limitations of surface stimulation can be at least partially circumvented by the use of electrode arrays. Individual activation of the pads in the array with adequate stimulation parameters permits defining an electrode with irregular shape that generates an optimized electrical field. Such optimization, in our case, will be devoted to having the best movement we can elicit, as defined by a figure of merit that will be presented below.

Therefore, this section presents an algorithm for selection of the optimal electrode geometry when eliciting a given movement with FES. Comfort issues will be also accounted for, since electrodes that evoke a painful sensation will be discarded. This study is motivated by the evidences gathered from both the Consortium's experience and the literature, and further supported by the results of our simulation study, as presented above. The algorithm is built upon other selectivity algorithms developed by partners of TREMOR Consortium [35, 36].

The **pad selection algorithm** proposed here starts by defining the stimulation parameters for which tonic contraction starts for each muscle group. For the sake of keeping this process to minimum duration, we keep the pulse duration and frequency constant, typically to 250 μs and 30 Hz. Then we increase in steps of 1 mA the stimulation amplitude (starting at 1 mA), until we achieve tonic contraction. In the second phase of the algorithm we stimulate each pad sequentially during 1 s with the previously selected parameters. A 2 s pause is allowed in between stimulations for the muscles to relax and the limb to return to its neutral position. Angular velocity is recorded with inertial sensors, in order to calculate the anatomical rotations generated by differential measurement [37, 38].

The optimal electrode geometry is defined as the ensemble of electrodes that provides the best movement, defined by the figure of merit K. This metric takes into account the amplitude of the desired movement, and

penalizes it with the displacement in undesired degrees of freedom. The figures of merit for wrist flexion/extension, adduction/abduction and forearm pronation supination are:

$$K_{ij} = \frac{1}{\theta_{fl/ext_{\max}}}\theta_{fl/ext} - \frac{1}{2}\left[\frac{1}{\theta^2_{pr/sp}}\theta^2_{pr/sp} + \frac{1}{\theta^2_{ab/ad}}\theta^2_{ab/ad}\right] \quad (1)$$

$$K_{ij} = \frac{1}{\theta_{ad/ab_{\max}}}\theta_{ad/ab} - \frac{1}{2}\left[\frac{1}{\theta^2_{pr/sp}}\theta^2_{pr/sp} + \frac{1}{\theta^2_{fl/ext}}\theta^2_{fl/ext}\right] \quad (2)$$

$$K_{ij} = \frac{1}{\theta_{pr/sp_{\max}}}\theta_{pr/sp} - \frac{1}{2}\left[\frac{1}{\theta^2_{ab/ad}}\theta^2_{ab/ad} + \frac{1}{\theta^2_{fl/ext}}\theta^2_{fl/ext}\right] \quad (3)$$

where i and j represent the position of the electrode as row and column in the array, $\theta_{fl/ext}$, the wrist flexion/extension angle, $\theta_{ad/ab}$, the wrist adduction/abduction angle, and $\theta_{pr/sp}$ forearm pronation/supination. Maximum achievable angles for each degree of freedom are represented by $\theta_{fl/ext_{\max}}$, $\theta_{ad/ab_{\max}}$, $\theta_{pr/sp_{\max}}$.

The output of the algorithm is the optimal electrode geometry (configuration of electrodes) to achieve a desired movement in a certain limb pose, and minimizing discomfort and pain. This configuration is immediately obtained by considering the electrodes with larger K. Only positive values are considered.

Next, we present **validation** of the proposed method. Two healthy subjects were stimulated with an array of 25 sewn electrodes, which were placed both on the wrist flexors and extensors; this array replicated in properties and geometry the first version of the active garment. The protocol was executed for two forearm poses, which are shown in Fig. 9(a) and (b). The arm was flexed in an angle around 90º, and the forearm was resting on an armchair. Inertial sensors were placed as shown in Fig. 9(c), to measure wrist and forearm rotations by differential measurement. A picture of the apparatus is shown in Fig. 9(d).

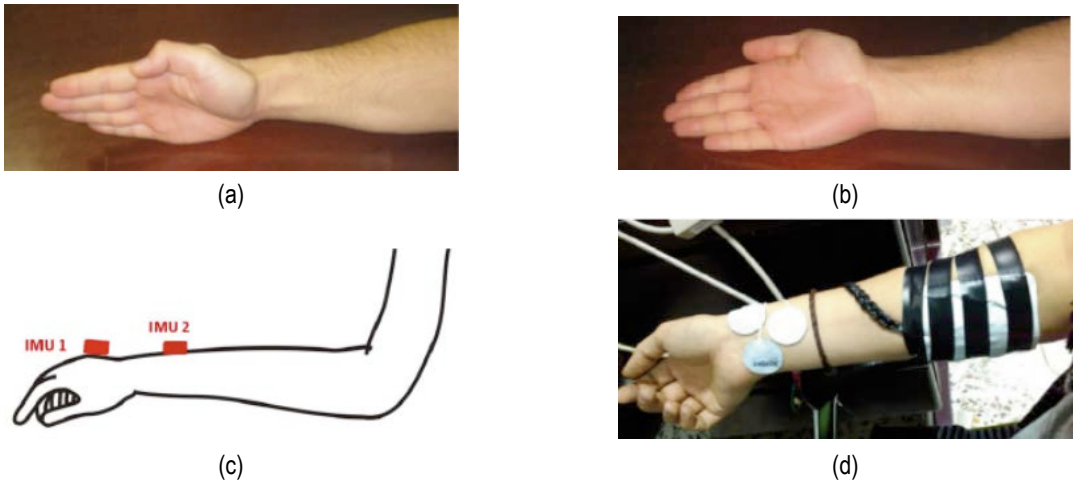

(a) (b) (c) (d)

Figure 9. Experimental validation of the pad selection algorithm: (a) and (b) arm poses in which the method was evaluated, (c) location of inertial sensors to measure the targeted rotations and (d) experimental apparatus.

After execution of the pad selection algorithm, the following electrode geometries were obtained. Fig. 10 shows the results for the two users in both limb poses. As expected, not only the electrode geometry to elicit two movements was different, but also to elicit the same movement in two forearm poses. This happens due to the relative displacement between muscles and stimulation surface when we rotate the forearm.

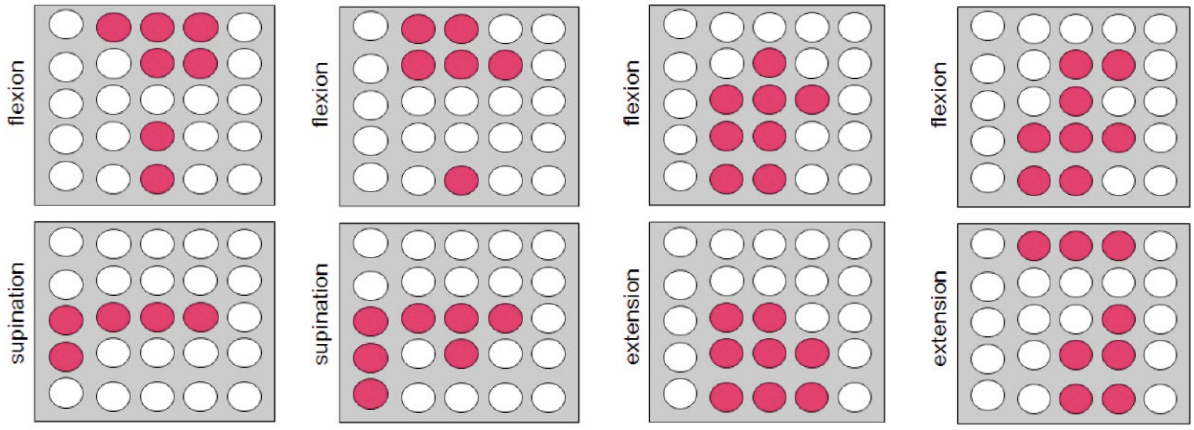

Figure 10. Results of validation of the electrode selection algorithm for two subjects and two forearm poses; two desired movements were elicited in each condition: (a) subject 1 in pose 1, (b) subject 1 in pose 2, (c) subject 2 in pose 1 and (d) subject 2 in pose 2. The elicited movement is indicated at the left side of the matrix. Active electrodes are coloured in magenta. The top part of the array corresponds to the proximal side of the forearm.

Moreover, the electrode geometry also depends on the stimulation amplitude. The injection of more current provokes deeper muscle contraction, and so macroscopic differences also appear. An example of this phenomenon is shown in Table II, where we can clearly observe that the "quality" of the evoked movement as defined by K varies considerably with the stimulation amplitude.

Metric K	Row	Column
0.59433	5	4
0.52029	5	3
0.50191	4	4
0.40019	4	3
0.33862	1	2
0.30749	1	3
0.29817	1	2
0.28702	3	0

(a)

Metric K	Row	Column
0.36369	4	2
0.34308	1	4
0.28743	3	2
0.27930	4	4
0.26398	4	3
0.25305	5	3
0.18335	2	4
0.15873	3	4

(b)

Table II. Influence of stimulation amplitude in electrode selection. The example corresponds to subject 2. In both cases the elicited movement is wrist extension, forearm pose is number #2. Stimulation amplitude: (a) 10 mA, (b) 8 mA; pulse duration and frequency were kept constant.

In summary, in this epigraph we have reviewed an experimental method to define the optimal electrode geometry to elicit different movements. Such method is quick to execute, allowing for calibration of the stimulation (electrode geometry and parameters) when a user dons the system on. The algorithm has been validated for different forearm movements in two poses, although has not been included in the control strategies since we are not using array electrodes due to the usability and comfort issues reported in the tests (see deliverable D8.2 for details). Implementation of this technique is, however, easy to carry out, and might be incorporated in follow-up studies.

1.2. Development of a plant model for FES based control

After reviewing the literature, one can find a considerable number of works dealing with more or less complex models for the control of FES systems. However, to our knowledge none of them deals with joint or muscle impedance, and most of the works in the literature require a detailed personalization [39, 40]. The former is fundamental to implement the semi-active strategy, while ease of identification is obviously very important for usability issues.

One of the most relevant studies on model-based FES control was conducted by Ferrarin *et al* [41]. The main drawback of this work indeed was the complexity of the system to be identified, since it considered electrical, physiological and mechanical parameters. Therefore the practical applicability of their approach was limited. Fig

11 shows their model, and one can observe the number of elements that affect the final motion. Such constituents are typically assimilated to black boxes for their identification.

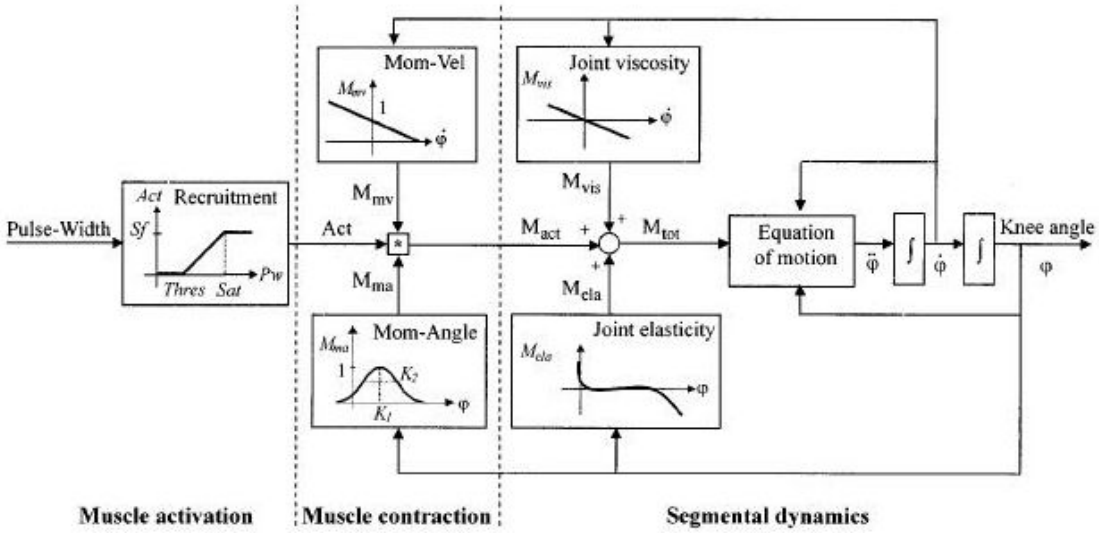

Figure 11. Physiological muscle model under FES proposed by Ferrarin *et al* [41].

It must be noticed that this model is already a simplification of that proposed in [40], not accounting for some physiologically relevant aspects such as muscle fatigue. As mentioned above, in spite of this simplification the identification of the system is yet time consuming and should be done every time the user wears the system.

According to this, we decided to develop a simple biomechanical model able to be used in a practical way by model-based tremor suppression controllers. The main principle is the batch identification of a second order linear system for different stimulations that elicit a certain movement. Validation for wrist extension and flexion is given

1.2.1. Model Overview

The model to be identified is a second order linear model in the form:

$$\omega(t) = a_1\theta(t) + a_2\alpha(t) + a_3 \tag{4}$$

where $\omega(t)$ represents the angular velocity of the limb, $\alpha(t)$ the angular acceleration and $\theta(t)$ the angular displacement; a_1, a_2 and a_3 are the coefficients to be identified.

Coefficients a_1, a_2 and a_3 are related to the physical parameters of the mechanical system according to:

$$T = k\cdot\theta(t) + c\cdot\omega(t) + I\cdot\alpha(t) \tag{5}$$

where k, c, and I represent the stiffness, damping and inertia of the joint respectively.

If we do a term-to-term identification we can establish the following relationships:

$$a_1 = -k/c \tag{6}$$

$$a_2 = -I/c \tag{7}$$

$$a_3 = T/c \tag{8}$$

As all the physical parameters must be positive, we constrain a_1, a_2 to be negative and a_3 to be positive. Since we have more variables that equations to proceed with the identification (3 equations and 4 variables to identify) we apply the Laplace Transform to (4) and rearrange terms to obtain:

$$\theta(s) = \frac{1/I}{s^2 + 2\xi\omega_n s + \omega_n^2}T(s) \tag{9}$$

We can therefore relate the natural frequency ω_n and damping factor ξ of the system to the parameters of (4) according to:

$$\omega_n = \sqrt{\frac{a_1}{a_2}} \tag{10}$$

$$\xi = \frac{-1}{2\sqrt{a_1 a_2}} \tag{11}$$

On the other hand, based on the fact that the inertia is constant for each individual we can re-arrange (4) into:

$$\alpha(t) = \frac{K}{I}\theta(t) + \frac{c}{I}\omega(t) + \frac{T}{I} \tag{12}$$

Finally, if we apply a series of 5 stimulation values for each targeted movement we can identify the relationship between the applied current C and the torque generated by the movement T or, at least the ratio torque inertia T/I that provides the overall transfer function of the movement.

1.2.2. Validation of the model

We recruited 9 subjects for the validation of the model. In total the user group comprised 5 healthy men and 3 healthy women and an essential tremor patient. The participants were comfortably sitting on a chair with armrest in neutral position, and had their hand fully extended and the wrist in neutral position in order to avoid the contribution of gravity. Two electrodes were placed on the forearm of the subjects, one over the belly of the extensor carpi radialis, the other one over the flexor carpi radialis; a common electrode was placed on the palmar or dorsal side of the wrist. Wrist movement was measured with two inertial sensors placed distally and proximally with respect to the wrist, also employing differential measurement [37, 38].

Angular acceleration and displacement were obtained by differentiation and integration of the angular velocity recorded from the gyroscopes. Differentiation was done using a local smoothing by a 5th order polynomial [42]. The integral has been directly computed from the cumulative sum.

As mentioned above, the protocol comprised five consecutive stimulations of 1 s duration for the identification of each movement, i.e. wrist flexion and wrist extension. A 2 s pause was allowed in between stimulation pulses.

In total 80 models were identified. Three of these models for two different subjects have a positive a_1 or a_2; therefore the 73 models left have physical meaning.

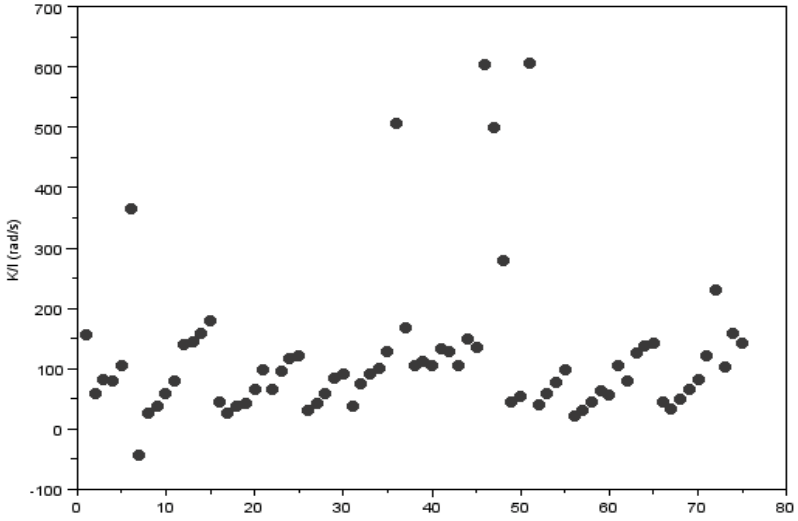

Figure 12. Estimated values of K/I for the 80 identified models (abscisa). This ratio should be proportional to the stiffness K of each subject given that there are no changes in the inertia I.

If we take a look at the obtained model coefficients, the ratio K/I (the first term in (12) that should be proportional to the stiffness since the inertia is constant) we can see in Fig. 12 that 7 measurements are over 200 rad/s, and one has a negative value. Notice that the 7 measurements with no physical meaning are included in this data set,

and that they occur always at the lowest possible stimulation amplitude for the user. Thus we conclude that system identification fails for very slow movements.

Fig. 13 shows that there exists a dependency between model parameters. As a matter of fact the stiffness and joint torque are linearly related.

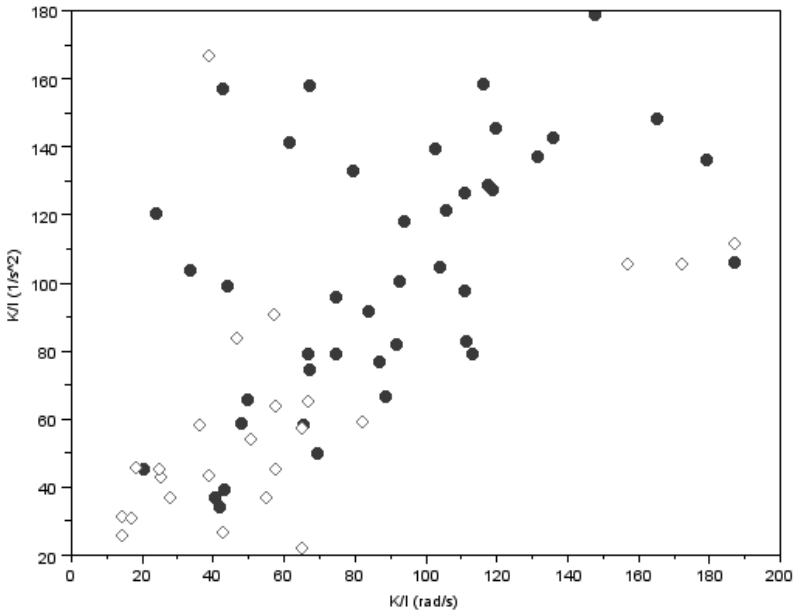

Figure 13. Relationship between torque and stiffness. Empty diamonds represent wrist extension, solid circles wrist flexion.

This linear dependency can be formulated as in (13). The stiffness component of the overall torque T_k is shown in (14).

$$\frac{K}{I} = m\frac{T}{I} + n \tag{13}$$

$$T_k = K \cdot \theta \tag{14}$$

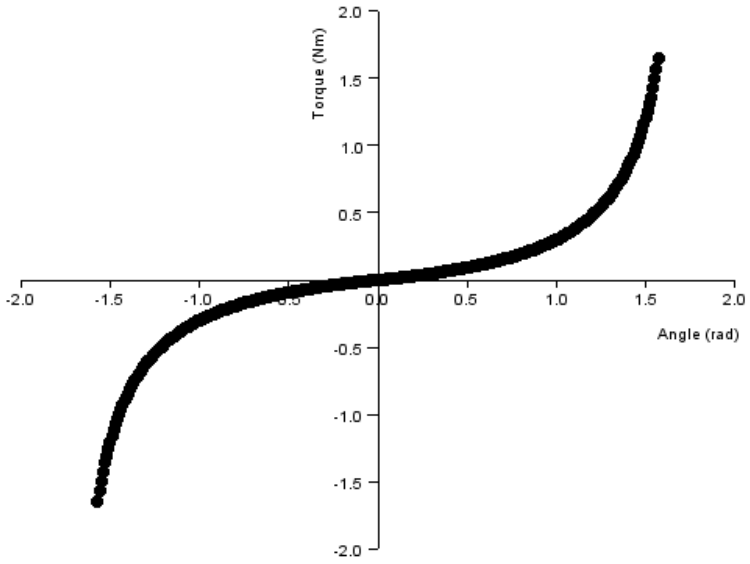

Figure 14. Mean stiffness identified from the models identified.

From these two equations we obtain:

$$T = \frac{n \cdot I \cdot \theta}{1 - m \cdot \theta} \tag{15}$$

Fitting this simple model with the data and considering an average inertia of 0.003 Nms^2/rad [43] the values for the linear regression are: m = 0.556 rad^{-1} and $n \cdot I$ = 0.133 Nm/rad. This relationship yields the curve shown in Fig. 14. The shape of such curve follows what is predicted from [41], and implies an overall motion range from the wrist of [-π/2, π/2] rad, as expected.

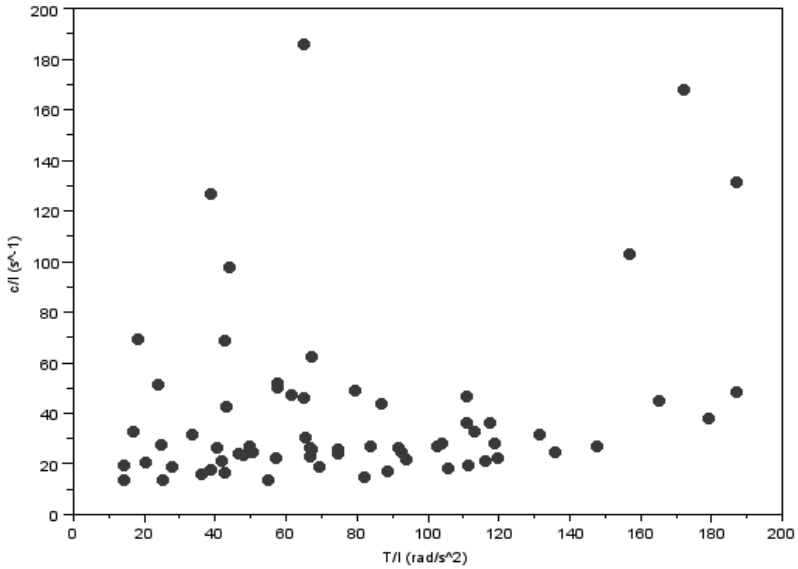

Figure 15. Relationship between torque and viscosity.

With respect to the viscosity parameter, Fig. 15 shows that there is no clear trend in the data, however the variance of this parameter is much higher than that of the stiffness. This is also in agreement with other methods reported for the estimation of viscosity. Table JMI summarizes the values of viscosity considering the same inertia we used for the stiffness.

Percentile 25	Median	Percentile 75
0.07	0.08	0.14

Table III. Summary of the values obtained for the viscosity coefficient considering a mean inertia of 0.003 N s^2 / rad.

From these data we can also obtain the physical parameters of the second order system defined in (9). Table JMII summarizes the values we have obtained.

	Natural frequency (ω_n)	Damping factor (ξ)
Percentile 25	7.0	1.2
Median	9.1	1.6
Percentile 75	11.1	2.3

Table IV. Physical parameters estimated for the model defined in (9).

The frequency response of the systems here identified resemble a low pass filter with a cut off frequency around 2 Hz, as shown in Fig. 16 for subject 1. Similar results are obtained for other subjects.

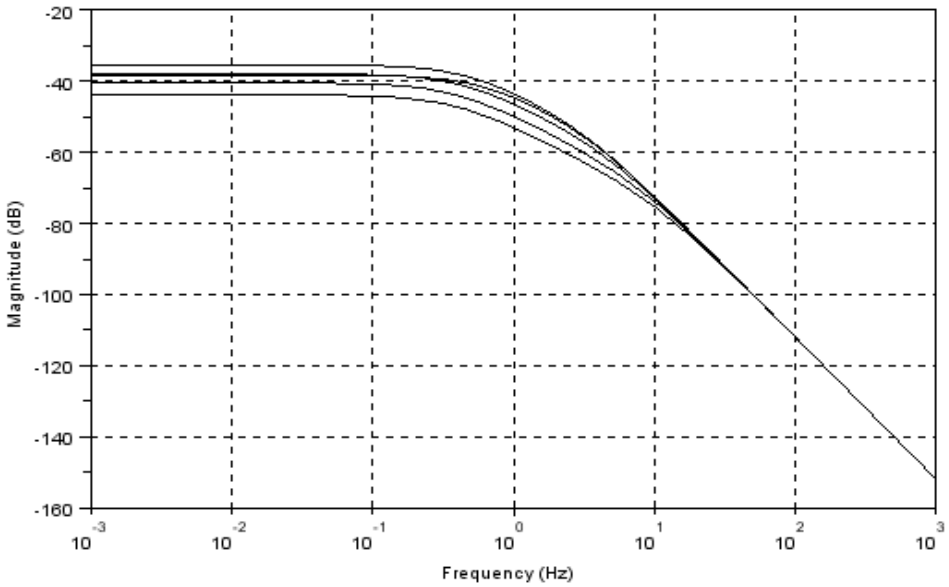

Figure 16. An example of the frequency response of the system identified. It corresponds to wrist flexion, subject 1.

Finally we can estimate the relationship between stimulation intensity and torque. Our results indicate that, as expected, the variance between individuals is high (which is in accordance with the need of individual calibration). Therefore, the stimulation intensity to achieve the same torque is very different, and comparing the flexor and extensor carpi radialis, the former requires much less intensity, Fig. 17.

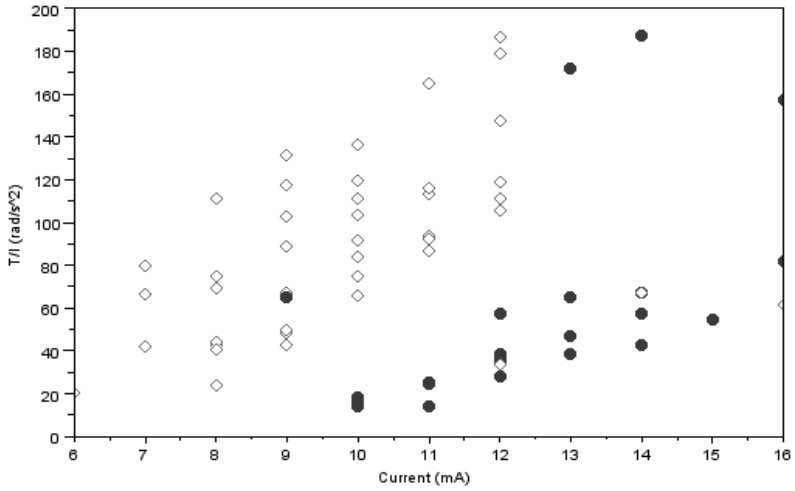

Figure 17. Relationship between the current intensity applied to the muscles and the estimation of generated torque elicited by each stimulation. Empty diamonds correspond to wrist flexion, solid circles to wrist extension.

The regression for each movement is summarized in Table V.

	Slope (N·m/mA)	Constant (N·m)
Flexion	0.0519	-0.217
Extension	0.0102	-0.003

Table V. Regression lines for the wrist flexion and extension movements. Relationship with stimulation intensity.

The most important aspect in the assessment of the model is, however, its ability to predict joint torque. As shown in Table VI the adjustment is usually very good for all the analysed movements; the model only fails in two of the movements analysed: extension in user 5 and extension in user 7.

User	Movement	Adjusted R^2
1	Flexion	0.88

2	Extension	0.90
2	Flexion	0.87
3	Extension	0.78
3	Flexion	0.96
4	Extension	1.00
4	Flexion	0.97
5	Extension	0.01
5	Flexion	0.79
6	Flexion	1.00
7	Extension	-0.23
7	Flexion	0.80
8	Flexion	1.00
9	Flexion	0.69

Table VI. Regression lines for the wrist flexion and extension movements. Relationship with stimulation intensity.

With the results above presented we are able to build a model of wrist flexion/extension under FES without the influence of gravity, Fig 18.

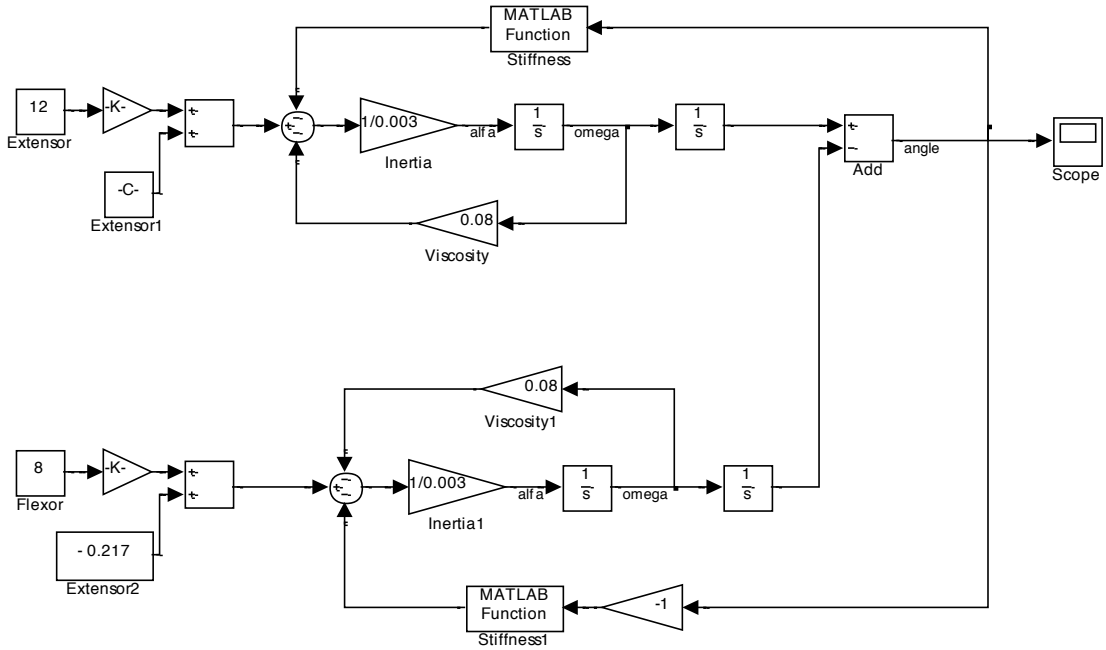

Figure 18. Block diagram of the identified physiological model of the wrist under electrical stimulation without the influence of the gravity component.

In conclusion, we have proposed and validated a method for the identification of a biomechanical model of the wrist, which, very importantly, can be identified in a reasonable time (~ 13 s per muscle) when the user wears the system. The model is suitable for being employed in a control loop such as has been done in [41]; as a matter of fact, this is foreseen as future work for the project as mentioned in next sections.

Moreover, in spite of its simplicity, the model reflects the main aspects accounted for in more elaborated approaches such as the nonlinearities of the torque-angular displacement relationship, and the parameters obtained are in agreement with the values reported in the literature.

2. Semi-active tremor suppression strategy

This section summarizes work on task WP6.2 "Development of a control approach for semi-active tremor suppression." This task is devoted to the development of a control algorithm that modifies the impedance of the muscles acting on a joint affected by tremor in order to filter it out. This objective has been addressed by developing and evaluating a number of versions of a controller that co-contracts the antagonist muscles that drive a joint, which in turn modifies its stiffness and viscosity.

CSIC led this task and collaborated with IBV in the different activities. A number of telemeetings and experimental sessions were held to coordinate the work. The output of this task was a controller that modifies the impedance of a joint and filters out the tremor without impeding the execution of a voluntary movement. The workflow we have followed was:

- Preliminary evaluation of co-contraction of antagonist muscles as a way to modify the impedance of a limb and attenuate the tremor. Such evaluation implied the development of a simple open-loop controller and its evaluation with a reduced group of patients.
- Development of the first version of the semi-active control strategy and evaluation with a group of users.
- Analysis of the outcome of this validation and integration of the major findings into a second version.
- Development of the second version of the semi-active control strategy and evaluation with a group of users. The major modifications included were modulation of the stimulation and the concurrent control of two joints.
- Analysis of the outcome of this validation and integration of the major findings into a third version.
- Development of the third version of the semi-active control strategy and evaluation with a group of users. This evaluation comprised both clinical and usability trials. The major modifications included were independent control of muscles and a more effective selection of stimulation parameters.

2.1. Background

The semi-active tremor suppression strategy is the first of the two control approaches developed and evaluated in the project. Such strategy is built upon two hypothesis: i) a human joint can be assimilated to a second order process, which frequency response resembles that of a low-pass filter [44], and ii) voluntary movements occur at a lower frequency that tremors [38]. Therefore, it is theoretically possible to place the cut off frequency of the filter in between the frequency at which the voluntary movement and tremor occur simply by changing the apparent impedance of the limb. Indeed a similar mechanism has been hypothesized to be naturally implemented in physiological conditions for limb stabilization [45, 46].

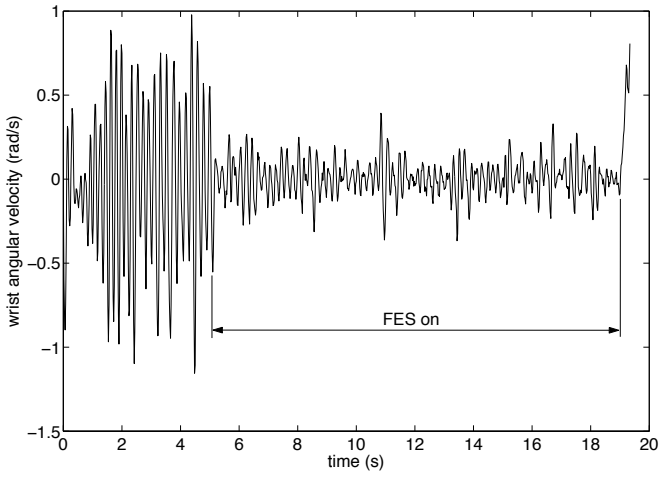

Figure 19. An example of the preliminary evaluation of tremor attenuation with the semi-active strategy. Open loop stimulation is applied to the wrist extensors and flexors; stimulation parameters are constant. The example corresponds to an essential tremor patient performing the finger-to-finger test. The data corresponds to wrist angular velocity (flexion/extension), the interval with FES is indicated by the line with arrows.

A dynamic increase of inertia is not possible in wearable systems for obvious reasons, but stiffness and damping can be controlled. As a matter of fact, this principle has been already implemented in various devices for tremor management using a number of technological approaches; e.g. in the WOTAS exoskeleton a constant damping was applied to the joint through conventional DC motors, attaining significant tremor attenuation [11]. Application

of impedance control for tremor suppression with FES is considerably novel; only one related publication has been recently published [14], and no experimental validation with tremor patients is given.

This section presents the semi-active tremor suppression strategy as it is implemented so far. As mentioned above three iterations of the controller have been carried out; all of them were evaluated with users, the outcome of the evaluation was included in the updated version of the controller, following the approach of iterative validation of partial components proposed in work package WP7.2. Moreover, first we carried out a few preliminary open loop experiments to validate the feasibility of the approach; an example is shown in Fig. 19.

2.2. First version of the semi-active strategy

A first version of the semi-active strategy was implemented and evaluated with users. As mentioned in the Executive Summary, the reader is referred to deliverable D8.2 "Case studies and analysis of functional, clinical and usability evidence of TREMOR system" for an exhaustive analysis of the results; here we will focus on the implementation of the strategy.

2.2.1. Strategy overview

This implementation was designed to further evaluate the feasibility of tremor management with FES, more specifically, trough impedance modulation. To this aim, we implemented a simple version of the strategy that co-contracted the agonist muscles acting on a joint in order to decrease the cut off frequency of the system and filter out the tremor. This is possible since application of FES may increase the apparent stiffness and viscosity of the joint. This first version applied a constant stimulation pattern when tremor was present; stimulation parameters were left constant, and chosen during an initial phase of calibration of the system on the user.

2.2.2. Experimental evaluation

Very briefly, the protocol implemented consisted in a number of 35 s trials, during which FES was applied if tremor was present between $time$ = 5 s and $time$ = 25 s. Like that, we obtained a recording of the tremor before stimulation and observed whether a permanent effect existed when FES was turned off. During the trial the patient was performing a clinical task designed to trigger the tremor. The same protocol was carried out for the active strategy. Indeed a number of repetitions without FES (to account for placebo effect), with the active strategy, and with the semi-active strategy were executed; experiment order was randomized. Regarding stimulation parameters, pulse duration and frequency were always fixed to 300 μs and 30 Hz; stimulation amplitude was identified for each muscle at the beginning of the session. The targeted degrees of freedom were wrist flexion/extension and elbow flexion/extension. The stimulation was driven by inertial sensors as foreseen in the DoW; four sensors were located as shown in Fig. 20 to characterize the desired movements by differential measurement [24, 25]. This configuration has been followed in all the experimental protocols presented hereafter.

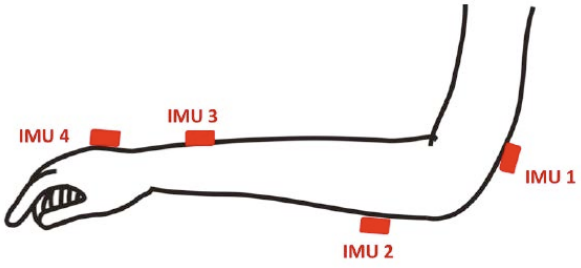

Figure 20. Location of inertial sensors to calculate wrist and elbow rotations by differential measurement.

Fig. 21 shows one of the best examples obtained with the semi-active strategy with this version of the strategy. The figure corresponds to an essential tremor patient, while executing an arms outstretched task to trigger the postural tremor. Attenuation is variable and goes from 50 % to negligible during the application of FES. No effects after turning off the stimulation are observed.

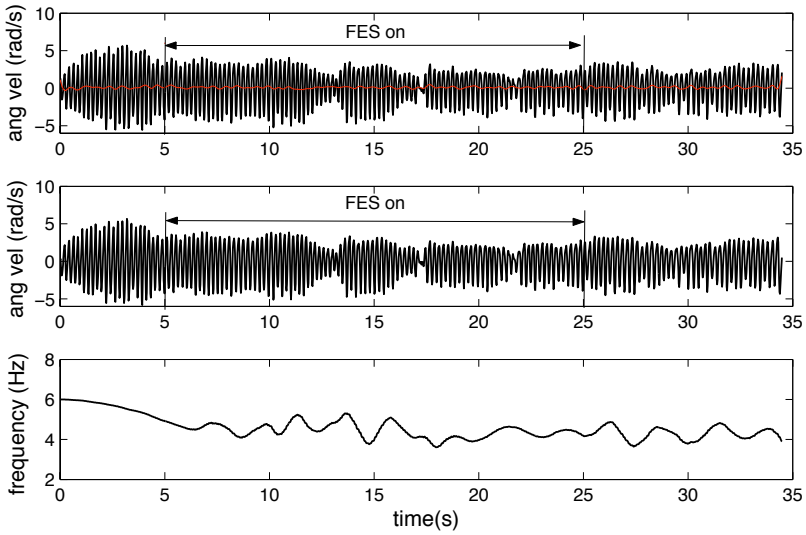

Figure 21. An example of tremor attenuation with the first version of the semi-active strategy. The example corresponds to an essential tremor patient executing an arms outstretched exercise. Intervals with and without FES are highlighted. The plots correspond to: Top: total wrist movement (black) and voluntary component (red), Middle: tremor component, and Bottom: estimation of tremor frequency. Analysis was performed online with the two-stage algorithm described in deliverable D4.1.

2.3. Second version of the semi-active strategy

2.3.1. Strategy overview

This new iteration of the semi-active strategy implements closed-loop modulation of the stimulation by controlling the current amplitude delivered to the antagonist muscle pair. Stimulation is updated in every tremor period as a function of tremor intensity at the targeted degree of freedom, thus independent joint control is implemented. The controller output is translated to stimulation parameters (amplitude) by means of a look up table (LUT) that is obtained during a previous calibration on the user; both muscles acting on the joint are updated based on the targeted impedance level. Impedance is manually identified by increasing the stimulation level on the antagonist muscles; details on this are given in the overview of the protocol below. The controller implemented in this version is a proportional controller, the gain is manually selected by the technician based on the relationship between tremor amplitude and stimulation amplitude; this is also explained below.

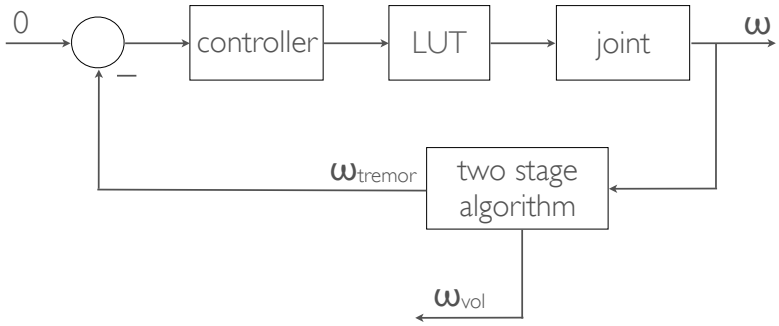

Figure 22. Block diagram of the second version of the semi-active strategy. This controller is implemented for each targeted degree of freedom (that coincides with an anatomical joint since in the project we target wrist flexion/extension and elbow flexion/extension).

Fig. 22 shows a block diagram that depicts this version of the semi-active controller for one degree of freedom. It consists in a very simple control loop that imposes a "zero tremor" reference to the user's joint (left). As mentioned above, the controller output is translated to stimulation parameters (current amplitude, pulse duration and frequency) based on a LUT that is identified on each user during the calibration phase. The variable fed-back to the controller is the tremor, which is extracted from the total joint movement by means of the two-stage algorithm [38] described in deliverable D4.1. The system is triggered when the onset of tremor is detected; this can be estimated from any source of information in a transparent manner for the controller.

The two-stage algorithm to characterize tremor from kinematic (inertial sensor) recordings is built on the well-known concept that, from a signal processing point of view, tremor and the concomitant voluntary movement are additive processes [47, 37, 38]:

$$x(k) = x_{tremor}(k) + x_{voluntary}(k) \tag{16}$$

where $x(k)$ represents the total joint movement, and $x_{tremor}(k)$ and $x_{voluntary}(k)$ the tremor and voluntary movement components respectively.

The voluntary and tremulous movements can be separated based on the fact that they happen in different frequency bands; tremors occur at a frequency between 3 and 12 Hz according both to the literature (e.g. see [48]) and our experiments, while the movements performed during activities of daily living involve wrist motion in a frequency range around 1 Hz, being the predominant frequency components between 0.48 and 2.47 Hz [49]. Therefore, we implemented a g-h filter that estimates the voluntary component of movement relying on its lower frequency.

$$x_{k,k} = x_{k,k-1} + g_k(y_k - x_{k,k-1}) \tag{17}$$

$$\dot{x}_{k,k} = \dot{x}_{k,k-1} + h_k(y_k - x_{k,k-1}) \cdot T_s^{-1} \tag{18}$$

$$x_{k+1,k} = x_{k,k} + T_s \cdot x_{k,k} \tag{19}$$

$$\dot{x}_{k+1,k} = \dot{x}_{k,k} \tag{20}$$

where (17) and (18) are the update equations, which estimate the future position and velocity of the state variable $x_{k,k}$ and $\dot{x}_{k,k}$ based on their previous predictions, and taking the current measurement y_k into account. In our case the state variable represents the voluntary movement. Confidence on the current measurement is weighed by gains g_k and h_k. Equations (19) and (20) are the prediction equations, and predict the future position and velocity $x_{k+1,k}$ and $\dot{x}_{k+1,k}$ based on a first order model of the process; $x_{k+1,k}$ is considered to be the estimation of voluntary movement.

The values of g_k and h_k are left constant and, related by (21); this implementation constitutes the so called critically dampened filter [50]. This relationship is derived from minimization of the square error of the previous measurements, weighing with less significance the oldest errors when integrating to estimate the error.

$$\begin{aligned} g &= 1 - \theta^2 \\ h &= (1-\theta)^2 \end{aligned} \tag{21}$$

It was explained at the beginning of this section that controller parameters are updated in every tremor period; therefore the instantaneous tremor frequency also needs to be estimated. In this case we employ a Weighted Frequency Fourier Linear Combiner (WFLC) to this aim. The WFLC is an algorithm widely used in similar contexts [51]. The WFLC is formulated as follows:

$$x_{r_k} = \begin{cases} \sin\left(r\sum_{t=1}^{k}\omega_{0t}\right), & 1 \le r \le M \\ \cos\left(r\sum_{t=1}^{k}\omega_{0t}\right), & M+1 \le r \le 2M \end{cases} \tag{22}$$

$$\varepsilon_k = s_k - \mathbf{W}_k^T \mathbf{X}_k - \mu_b \tag{23}$$

$$\omega_{0_{k+1}} = \omega_{0_k} + 2\mu_0 \varepsilon_k \sum_{r=1}^{M}\left(w_{r_k} x_{M+r_k} - w_{M+r_k} x_{r_k}\right) \tag{24}$$

$$\mathbf{W}_{k+1} = \mathbf{W}_k + 2\mu_1 \varepsilon_k \mathbf{X}_k \tag{25}$$

where (22) represents the harmonics of the Fourier series that estimates the tremor, (23) the error to be minimized by the LMS algorithm [52], and (23) and (24) the amplitude and frequency adaptation. The WFLC has four parameters to tune: μ_0 and μ_1 the amplitude and frequency gains, μ_b an offset to compensate for low frequency bias, and M the number of harmonics. The input signal, s_k, is the tremor estimation derived from (16) and (19). The initial frequency of the filter can be obtained either from current surface EMG data, or more simply

from the inertial sensors. The latter implementation was preferred in order to minimize setup time, and test a system that follows a more "product-like" approach. Therefore, tremor frequency was estimated directly from the amplitude spectrum after tremor onset, which is detected by applying a threshold to the tremor component of movement $x_{tremor}(k)$. We employ a simple 2 s window to calculate the amplitude spectrum, in order to double-check the detection of tremor onset we use the following criterion that relies on the spectral characteristics of the total movement: if the tremor to voluntary movement (TVR) ratio is larger than a certain value obtained experimentally, then we consider the spectrum to reflect tremor. In case this condition is not fulfilled, another 2 s window is considered; 1 s overlapping is allowed. The TVR is defined as in (26). Similar ratios have been employed in the literature of tremor for EMG analysis (see e.g. [53]).

$$TVR = \frac{\sum_{f=3}^{f=12} X_f}{\sum_{f=0}^{f=3} X_f} \tag{26}$$

where $\sum_{f=0}^{f=3} X_f$ and $\sum_{f=3}^{f=12} X_f$ represent the integral of the amplitude spectrum for the 0-3 Hz and 3-12 Hz bands.

Once we have an estimation of the tremor and its instantaneous period duration, the control action is updated by means of a simple proportional law:

$$u(k) = K_p \overline{x}_{tremor}(k) \tag{27}$$

where $u(k)$ represents the controller output, K_p the proportional gain and $\overline{x}_{tremor}$ the tremor intensity defined as the amplitude in the last period. Therefore, the output of the controller for a given period is adapted according to the tremor parameters estimated in the last period, which gives the controller a predictive nature.

Finally, the controller output $u(t)$ is translated to stimulation parameters by means of a LUT, Fig.22. The LUT relates a certain tremor intensity to a couple of current values, one for each antagonist muscle acting on the joint.

Notice that the estimation of tremor frequency is compared with the real frequency (of the last period) obtained by calculation of the zero-crosses; if the prediction has an error of more than 20 ms the controller output is not updated. This criterion is imposed since tremor frequency is almost constant during an exercise (according to out data and the literature, e.g. [11, 54]) and abrupt variations correspond to situations were tremor has almost disappeared or, more rarely to unexpected and brusque changes induced by a controller malfunctioning. If the prediction and the real period duration do not coincide for more than 10 real periods the controller is restarted.

2.3.2. Experimental evaluation

As stated at the beginning of this section, this strategy was evaluated with patients following the iterative approach proposed in the project. The experimental protocol comprised two major phases: i) the calibration of stimulation parameters for the user, and ii) the tremor suppression experiments. As for the previous experiment, the tests consisted in selecting an exercise that triggered the tremor and comparing the performance of this strategy with that of the active strategy. Recordings without FES and with sensory stimulation were considered to account for a possible placebo effect. Again, trials were randomized; wrist flexion/extension was the targeted movement. Regarding stimulation parameters, pulse duration and frequency were always fixed to 250 μs and 30 Hz or 300 μs and 40 Hz depending on the musculature of the user; current amplitude was adapted by the controller after calibration on each user. A similar approach was used in [14], where stimulation frequency and amplitude were constant, and the controller modulated the pulse duration.

The calibration consisted in estimation of the stimulation amplitude to co-contract the antagonist muscles and attain an increase on limb impedance. Typically five levels were visually identified per user and joint. These levels were then fed to the controller, and defined the LUT.

Controller parameters were: θ was fixed to 0.900, μ_0 to 0.001, μ_1 to 0.01, μ_b to 0.01, and M to 1; these values were the same for all the users, since they depend only on the kinematics of voluntary and tremulous motion. K_p was personalized based on visual inspection of the tremor severity during calibration and the average stimulation amplitude required to elicit a similar motion. Tremor onset was detected by applying a threshold to the tremor component of the movement ($x_{tremor}(k)$ > 0.1 rad/s); the WFLC was initialized also based on movement information, using the TVR as defined in (26), the condition TVR > 3 is imposed.

Next we show a step-by-step example of tremor suppression with this version of the semi-active strategy. The example corresponds to one of the best trials with an essential tremor patient during a rest task. First, Fig. 23 shows the online estimation of voluntary movement and tremor. The online estimation of tremor is employed to calculate the intensity per period; period duration is immediately derived from the instantaneous frequency.

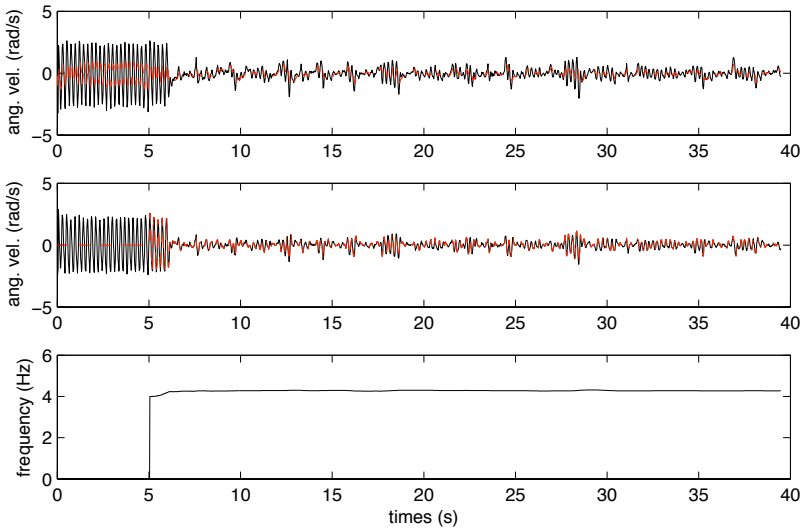

Figure 23. Estimation of tremor amplitude and frequency by the controller implemented in the second version of the semi-active strategy. The example corresponds to an essential tremor patient performing a rest task. Top: raw wrist rotation (black) and estimation of volitional component (red); Middle: tremor obtained off-line for comparison sake (black) and online tremor estimation (red) –this estimation is used to extract severity; Bottom: online estimation of tremor frequency.

Fig. 24 shows the instants at which the tremor estimation crosses zero, which indicates a change of anatomical sense of rotation (wrist extension is positive), and the controller output. In this example tremor is attenuated (*time* ~ 6 s) to almost zero amplitude when stimulation is turned on. Afterwards, the controller is not updated for *time* ~ 3 s since the estimated instantaneous tremor frequency is very different to the real one; as a matter of fact, the amplitude of the tremor component resembles the white Gaussian noise inherent to the inertial sensors. Next controller update restarts.

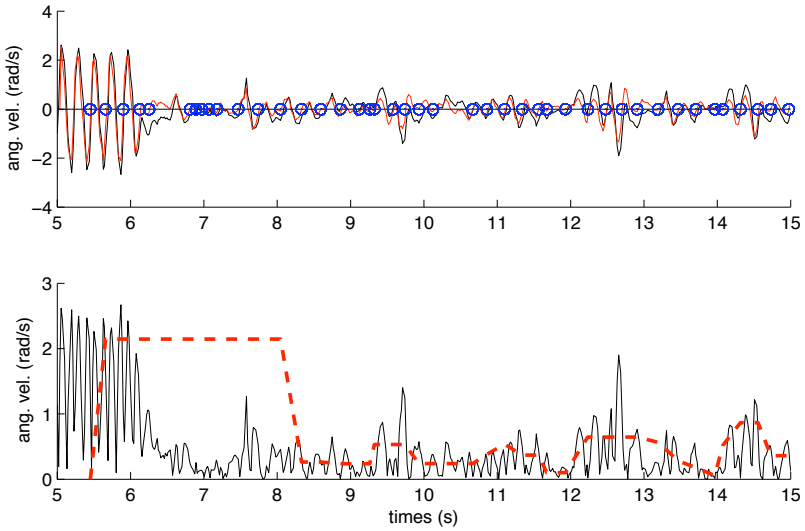

Figure 24. Estimation of tremor amplitude and real frequency (zero-crosses) by the controller implemented in the second version of the semi-active strategy. The example corresponds to an essential tremor patient performing a rest task (same as Fig. 23). Top: wrist rotation (black), tremor estimated online (red) and zero crosses obtained online (blue circles); Bottom: rectified wrist motion (black) and controller output (red dashed line).

Fig. 25 shows the resultant stimulation patterns after conversion of the controller output with the LUT identified during calibration. Considerable tremor suppression is obtained once stimulation is on. Notice that when tremor is completely attenuated (e.g. *time* ~ 18 s) the stimulation amplitude becomes 0, and tremor quickly reappears, which in turn triggers again the stimulation. This behaviour was observed only in some patients, in others the hand stayed stabilized for a few seconds. A more thorough discussion on this will be given in deliverable D8.2.

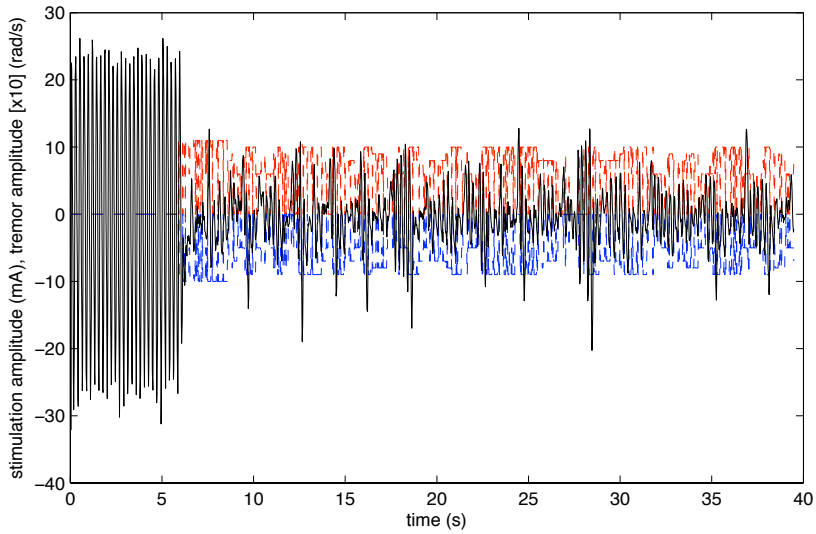

Figure 25. Attenuation of tremor with the second version of the semi-active strategy. The example corresponds to an essential tremor patient performing a rest task (same as Fig. 23). The plot shows the online estimation of tremor (black) and the stimulation patterns for wrist extensors (red) and flexors (blue). Tremor amplitude is scaled [x 10] for visualization sake.

2.4. Third version of the semi-active strategy

2.4.1. Strategy overview

This section details the implementation of the last version of the semi-active strategy. This version implements the following major changes with respect to the previous one: i) each muscle acting on a joint was controlled independently, ii) the LUT was replaced by a saturation function that translated the controller output into muscle activation, and iii) an integral term was included in the control law.

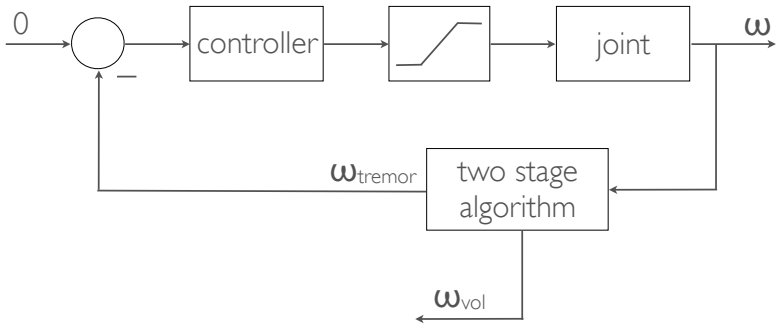

Figure 26. Block diagram of the third version of the semi-active strategy. This controller is implemented for each targeted muscle; therefore two independent controllers drive each anatomical joint.

Regarding the first two modifications, during the validation of the second version of the semi-active controller it was observed that during continuous stimulation the response of the antagonist muscles changes, which makes the relationships established in the LUT more inaccurate than first expected. This effect is more evident for the elbow joint, as revealed by experiments carried out in control subjects. The reason for this is the considerable difference in volume and hence in number of fibres and physiological properties of the biceps brachii and the lateral head of the triceps –the simple effect of muscle fatigue tends to provoke an elbow flexion after a few seconds of continuous co-contraction. Finally, from a control engineering perspective it seems more natural to consider each muscle as an “actuator” that elicits a certain movement (flexion or extension), rather than considering both actuators to be coupled systems that generate a movement. Therefore, we decided to control independently each muscle, and to avoid the use of a fixed current amplitude-elicited movement relationship (the

LUT), but just a simple linear transfer function with saturation. The saturation is implemented in order to prevent the stimulation level of exceeding a certain comfort level identified during calibration.

As for the third modification, the integral term is included to account for the abovementioned non-stationary response of the muscle to stimulation. In previous experiments it was observed that simple proportional control sometimes did not provoke a co-contraction level sufficient to filter out the tremor, therefore we hypothesized that an increase of the control action by integration of the error (i.e. tremor amplitude, see Fig. 22) might circumvent this issue. The final control loop is shown in Fig. 26, the only difference with respect to version two is that one controller is now implemented per muscle not per joint, and the LUT has been replaced by a transfer function with saturation.

In more detail, the controller is implemented as follows. Modulation of stimulation is based on the same estimation of tremor reviewed in the previous section. Next the controller (described below) provides a certain control action that is translated to a stimulation command by the linear transfer function with saturation. Again, the stimulation is triggered after tremor onset is detected (from any sensor modality), the initial frequency can also be extracted from surface EMG or inertial sensors. The former approach also relies on calculation of the TVR, (26).

The controller is not a single control law, but rather a "controller scheduling" scheme is implemented. This approach consists in a series of rules to choose among three controllers. The reason for this is, as we mentioned in the second version of the controller, that if the real duration of a tremor period is not in agreement with the prediction (or if the error was larger than 20 ms) a special event might be occurring; such event can be either the complete attenuation of the tremor, or a brusque unexpected movement. Notice that the underlying hypothesis for this is that tremor frequency is almost constant [54], and not altered when biomechanical loads are applied [11, 13]. This mechanism is further exploited in this version as follows:

IF frequency error IS less than 100 ms THEN proportional-integral control is used
IF frequency error IS between 100 ms and 500 ms THEN proportional control is used (28)
IF frequency error IS larger than 500 ms THEN no control action is applied.

Like for the previous version, the rules are reset after a number of real tremor periods with large frequency estimation error. The number of periods is fixed to 15.

The proportional-integral controller is implemented as follows; the proportional controller is defined in (27).

$$u(k) = K_p \bar{x}_{tremor}(k) + K_i \sum_{j=1}^{k} \bar{x}_{tremor}(k)\Delta t \tag{29}$$

where $u(k)$ represents the controller output, K_p the proportional gain, K_i the integral gain, Δt the sampling period, and $\bar{x}_{tremor}$ the tremor intensity defined as the amplitude in the last period. The integral is reset to avoid saturation when the amplitude of the tremor goes below 0.4 rad/s.

The controller output is then fed into a transfer function that yields the stimulation amplitude, Fig. 26. As explained above, this function is identified during a previous calibration phase; a saturation fixed to a level that corresponds either to the discomfort threshold, or to a contraction that elicits a very quick movement with high amplitude defines the maximum stimulation to be delivered. The minimum stimulation level is simply fixed to 0.

2.4.2. Experimental evaluation

Again this strategy was evaluated in patients following the iterative approach envisioned for the integration of partial components. Both clinical and usability tests were performed to validate this strategy; extensive details on them are given in deliverable D8.2. Here we summarize the protocol used during the clinical validation and give an illustrative example to show the performance of the controller. Again, the experimental protocol comprised two major phases: i) the calibration of stimulation parameters for the user, and ii) the tremor suppression experiments. As for all the clinical trials, the tests consisted in selecting an exercise that triggered the tremor and comparing the performance of this strategy with that of the active strategy. Sensory stimulation was also considered. Stimulation was delivered to the wrist extensors and flexors and to the biceps and triceps; thus, two degrees of freedom were controlled. Again, stimulation was amplitude modulated, pulse width and frequency were kept constant, and chosen based on the same criteria.

The calibration aimed at finding the maximum stimulation intensity for each muscle group during co-contraction. We proceeded as follows: first we looked for the maximum amplitude during independent muscle stimulation, and then starting from the 75 % of these maxima we looked for the maximum values during co-contraction. This

amplitude defined the saturation level in the controller for every muscle. The process is simple and quick, and might be automatized in the future.

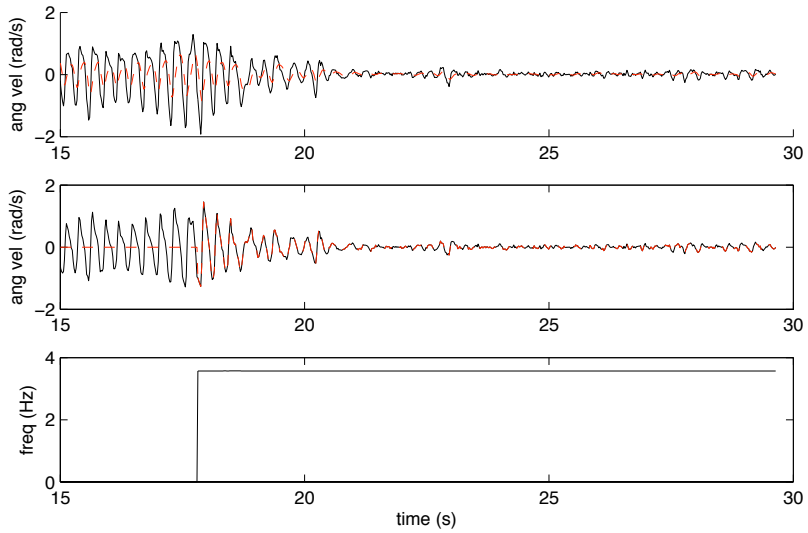

Figure 27. Estimation of tremor amplitude and frequency by the controller implemented in the third version of the semi-active strategy. The example corresponds to a patient suffering from Parkinson's disease performing a finger-to-finger test. Top: raw wrist rotation (black) and estimation of volitional component (red); Middle: tremor obtained off-line for comparison sake (black) and online tremor estimation (red) –this estimation is used to extract severity; Bottom: online estimation of tremor frequency.

Controller parameters were left to the same values than in the previous version, the integral gain K_i was also personalized based on visual inspection. Tremor onset was also obtained from movement data; both muscles acting on the elbow and on the wrist were triggered at the same time, although the stimulation was only triggered for the tremulous joint(s). The TVR served to initialize the WFLC; we also used the criterion TVR > 3 to ensure adequate detection of volitional motion.

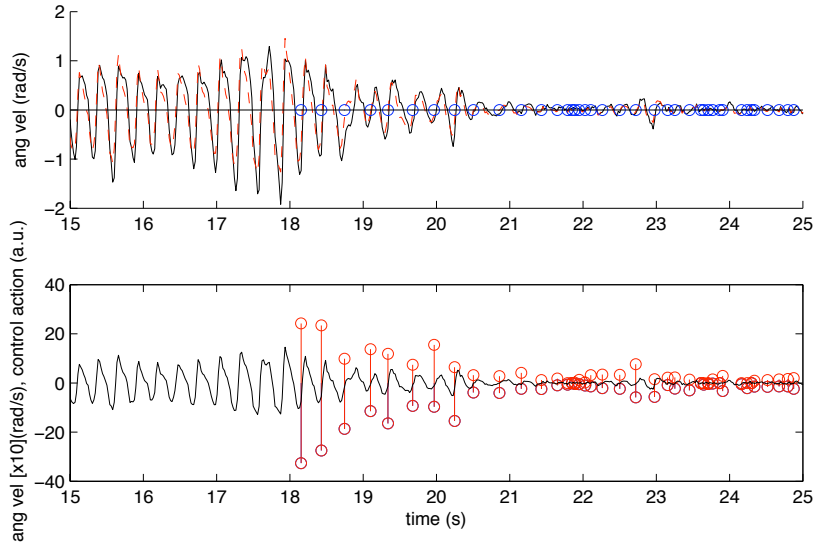

Figure 28. Estimation of tremor amplitude and real frequency (zero crosses) by the controller implemented in the third version of the semi-active strategy. The example corresponds to a patient suffering from Parkinson's disease performing a finger-to-finger test (same as Fig. 27). Top: wrist rotation (black), tremor estimated online (red) and zero crosses obtained online (blue); Bottom: tremor estimated online (black) and control output per period (red). A wrist extension is represented as positive; the control output follows the same convention.

Here we show a step-by-step example of this version of the controller. It is one of the average trials with a Parkinson's disease patient during a postural task, i.e. the so-called finger-to-finger test. Fig. 27 shows the decomposition of wrist rotation into voluntary movement and tremor; the algorithm is the same employed in the

second version of the controller. Tremor frequency shows very low variation with FES; considerable attenuation ($time$ ~18 s, when frequency estimation starts) is achieved.

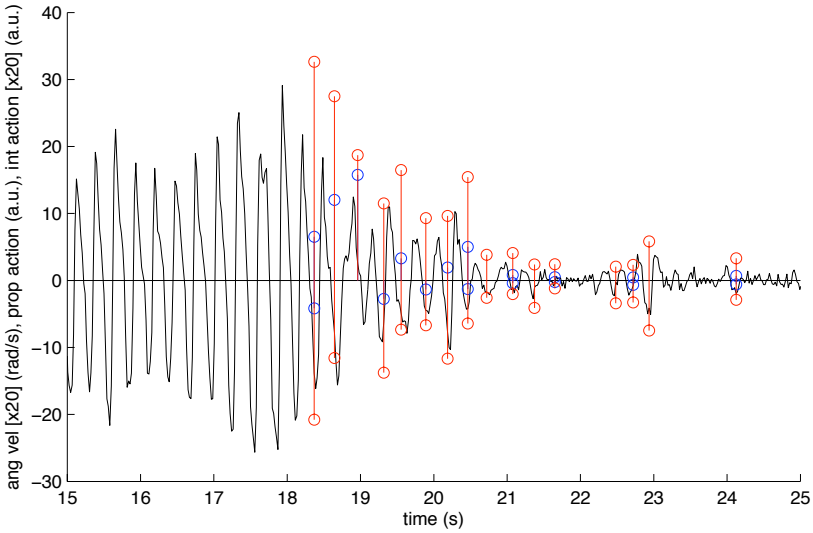

Figure 29. Proportional and integral terms for the controllers of wrist extensors and flexors with the third version of the semi-active strategy. The example corresponds to a patient suffering from Parkinson's disease performing a finger-to-finger test (same as Fig.27). The plot shows the online estimation of tremor (black) and the proportional (red) and integral (blue) components of the control action. The control actions (discrete values) are represented when they are first applied, i.e. at the beginning of a tremor period. A positive action corresponds to wrist extensors, a negative to flexors. Tremor amplitude and the integral term are scaled [x 20] for visualization sake.

Fig. 28 shows the instants at which tremor amplitude crosses zero, which indicates a change of anatomical rotation (wrist extension is positive), and the outputs of the controllers for the extensors and flexors. The output of the extensors controller is driven by the severity in flexion, and conversely the output of the extensors controller is modulated as a function of wrist extension. We observe that when tremor is completely attenuated by the stimulation, the control output becomes zero ($time$ ~ 21.6 s). Moreover, this also causes that the estimated frequency is very different to the real one, which justifies the rules defined in (28). On the other hand, visual inspection indicates that the relationship between the control outputs for the extensors and flexors is not constant, therefore supporting implementation of independent controllers for antagonist muscles.

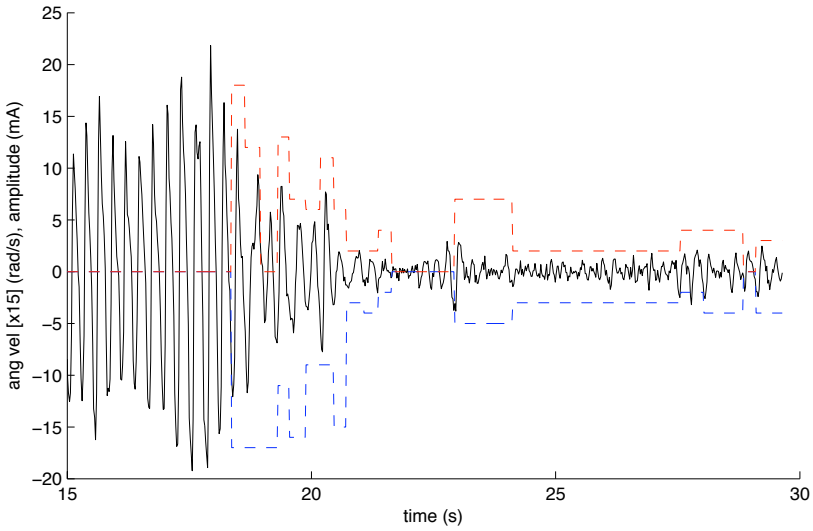

Figure 30. Attenuation of tremor with the third version of the semi-active strategy. The example corresponds to a patient suffering from Parkinson's disease performing a finger-to-finger test(same as Fig. 27). The plot shows the online tremor estimation (black) and the stimulation patterns for wrist extensors (red) and flexors (blue). Tremor amplitude is scaled [x 10].

Fig. 29 details the contributions to the control action of the proportional and integral terms. If we look at the control action that corresponds to wrist extensors (positive in the figure) we observe that during the first three tremor periods the integral term is adding to the total output, but when tremor in flexion descends below a threshold (0.4 rad/s) the integral is reset ($time$ ~ 19 s, i.e. no integral action is applied in the fourth stimulation period). The effect of the integral term is more dramatic in cases where no attenuation is attained, since it rapidly increases the control output to saturation level.

Finally, Fig. 30 shows the resultant stimulation patterns after conversion of the outputs of the controllers for the flexors and the extensors. Considerable tremor suppression is obtained once stimulation is on. As happened for the second version of the strategy, when tremor is completely attenuated ($time$ ~ 22 s) the stimulation amplitude becomes 0, and tremor reappears, which in turn triggers again the stimulation. In this patient, after tremor is significantly suppressed the limb tends to exhibit a more stable behaviour, and low co-contraction levels are capable of preventing severe tremor from reappearing. A more thorough discussion on this will be given in deliverable D8.2.

In **conclusion**, we have developed a semi-active control strategy that modifies joint impedance by co-contraction of the antagonist muscles. Individual control of muscles acting on a joint permits the system adapting to the intrinsically non-stationary muscle response under FES. Moreover, proportional-integral control enhances this rapid adaptation both to user's accommodation to stimulation and the realization of different activities, and optimizes the output of the controller. Such controller is not model-based but instead is driven by the dynamics of the tremor. Inclusion of a model in a model-based adaptive impedance controller is identified as future work.

3. Active tremor suppression strategy

This section describes the activities on task WP6.3 "Development of a control approach for active tremor suppression." This task aims at developing a control algorithm that drives the muscle out of phase with respect to the tremor, in order to attenuate it. As for WP6.2, we have addressed this objective by developing and evaluating a number of versions of a controller that generates an oscillation with similar amplitude and frequency but opposite frequency that counteracts the tremor.

CSIC led this task and collaborated with AAU, UNA and IBV in the different activities. A number of telemeetings, research visits and experimental sessions were scheduled to coordinate the work. The output of this task was a couple of controllers that employ out of phase stimulation to alleviate the tremor. The work was organized as follows:

- Preliminary evaluation of the feasibility of generating oscillations with different amplitudes and frequencies. Tests on a representative group of control subjects were carried out.
- Development of the first version of the active strategy and evaluation with a group of users.
- Analysis of the outcome of this validation and integration of the major findings into a second version.
- Development of the second version of the active control strategy and evaluation with a group of users. The more significant improvements were modulation of the stimulation and the simultaneous control of two joints.
- Analysis of the outcome of this validation and integration of the major findings into a third version.
- Development of the third version of the active control strategy and evaluation with a group of users. The major modifications included were independent control of antagonist muscles and a more effective selection of stimulation parameters.

These activities correspond to the active strategy driven by inertial sensors as foreseen in the DoW. FES control relying entirely on kinematic recordings was considered due to the artefacts that stimulation generates in EMG recordings. However, in parallel, the TREMOR Consortium has explored an alternative version of the active strategy that relies on surface EMG alone. The reason for this is that selection of stimulation sites and FES control in this approach is more critical than for the semi-active strategy, and hence direct assessment is expected to be beneficial.

It must be noticed that every one of the three versions of the active strategy was tested in the same experimental sessions that the semi-active strategy. Moreover, as mentioned in the Executive Summary, the reader is referred to deliverable D8.2 "Case studies and analysis of functional, clinical and usability evidence of TREMOR system" for an exhaustive analysis of the results; here we will focus on the implementation of the strategy; only an illustrative example will be given.

3.1. Background

The active tremor strategy is the second control approach developed and evaluated in the project. This strategy is also relies on the idea that tremors and voluntary movement occur at different frequencies, and therefore notch filtering at tremor frequency is possible. Such notch filter is physically implemented through out of phase stimulation [11]; precise frequency tracking and phase selection is fundamental.

As a matter of fact this strategy was already implemented in Prochazka and colleagues' seminar work [12]. There, the authors used a displacement sensor mounted on a table and surface electrodes to characterize the impedance of the user's wrist, and in turn design a notch filter that interfered as little as possible with voluntary movements, defined to be in the 0-1 Hz range. This system was evaluated with a group of 24 patients suffering from the major types of tremor, achieving significant attenuation for all of them: 73 % for essential tremor, 62 % for Paskinson's disease and 38 % for cerebellar tremor. Therefore, this study demonstrated the feasibility of such approach, although it must be noticed that the experimental apparatus greatly constrained the implementation of the authors' approach into a daily living system.

Only another group apart from the TREMOR Consortium has investigated an active approach to tremor suppression with FES. In their study, the authors combine surface EMG and accelerometer recordings in order to estimate the frequency and phase of the tremor and generate an out of phase movement. At the present time, they have not published results exploiting the amplitude of the tremor. Moreover, their experimental results they have presented so far are only from a single essential tremor patient [15]. However, they have implemented an interesting methodology to remove stimulation artefacts –although it implies constraining the stimulation frequency– [55] and to account for the electromechanical delay in their control loop [56].

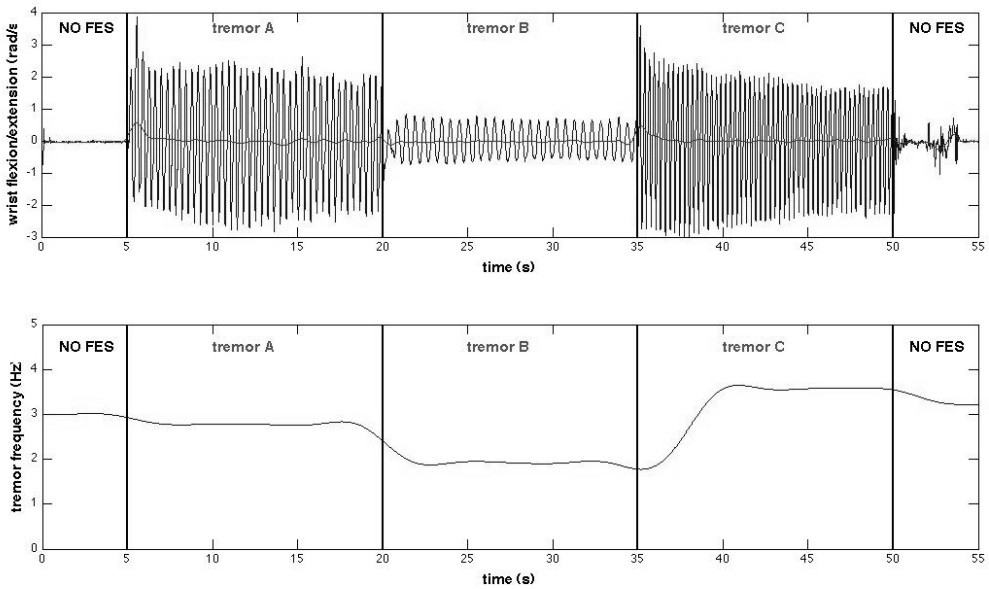

Figure 31. Elicitation of a tremor-like oscillation in a control subject. The top plot shows wrist flexion/extension, the bottom plot the online estimation of frequency. The desired tremor characteristics were: tremor A: frequency: 3 Hz, amplitude: 2 rad/s; tremor B: frequency: 2 Hz, amplitude: 0.8 rad/s; and tremor C: frequency: 4 Hz, amplitude: 2 rad/s.

This section presents the active tremor suppression strategy as it is implemented so far. As mentioned above three iterations of the controller have been carried out; all of them were evaluated with users, the outcome of the evaluation was included in the updated version of the controller, following the approach of iterative validation of partial components proposed in work package WP7.2. Apart from these activities, the alternative implementation of the strategy relying on surface EMG as sensory input is summarized. Notice that neither of these strategies implements a model of joint impedance to optimize the filter.

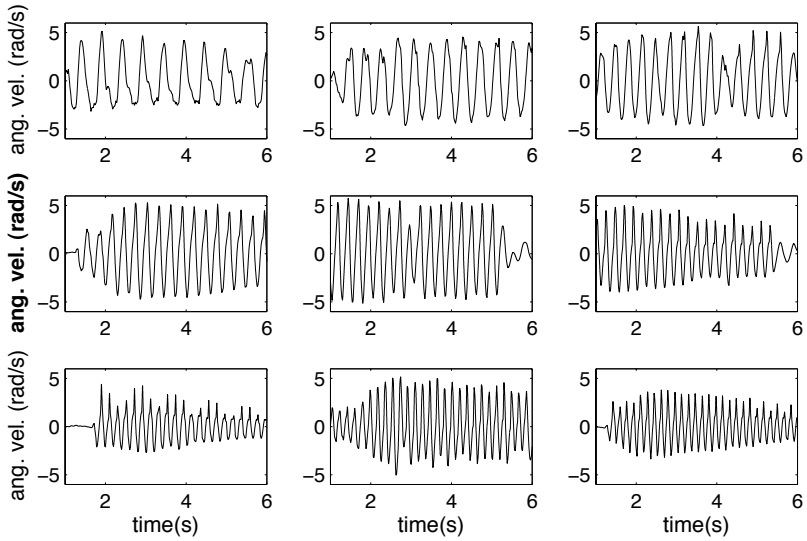

Figure 32. Elicitation of a tremor like oscillation in a control subject. The reference tremor input frequency is (from top left to bottom right): 2, 2.5, 3, 3.5, 4, 4.5, 5, 5.5 and 6 Hz. Stimulation amplitude was left constant after manual calibration.

Before presenting the different implementations of the active tremor suppression strategy, we will briefly summarize our preliminary study on generation of oscillatory movements that resemble tremor, which is the practical basis for implementation of this strategy. Fig. 31 shows that we can generate a tremor-like oscillation in control subjects, and that control of its characteristics, i.e. amplitude and frequency, is possible. This example demonstrates that we can accurately generate oscillatory movements with different frequencies, since the reference frequency matches the online estimation (bottom). Nevertheless, for tremor C we observe a decay in amplitude, as a consequence of rapid fatigue. This illustrates the need of adapting the stimulation parameters.

Fig. 32 illustrates that fine frequency control is achievable; it illustrates nine examples in steps of 0.5 Hz. The example also corresponds to a control subject. Our conclusion is that, as expected, it is feasible to implement an active tremor strategy based on FES. It must be noticed that the highest frequency reported in the literature for this application is 5.4 Hz [13]; thus we wanted to ensure the possibility of generating a larger span of frequencies.

3.2. First version of the active strategy

3.2.1. Strategy overview

This section summarizes the implementation of the first version of the active strategy. As for the first version of the semi-active strategy, this controller was implemented to evaluate the feasibility of tremor management with a notch filter, as shown in the literature [12, 13]. This first implementation relied only on the frequency tracking algorithm described in subsection 2.2; the frequency estimation yielded by (24) was used to predefine the frequency at which the stimulation should switch from one muscle to another. The sign of the tremor estimation obtained from (16) served to control the phase. Zero crosses of the tremor component of movement (also given in (16)) were employed to correct the frequency estimation; i.e. to switch the muscle to stimulate. No modulation of the current density generated by the stimulation was implemented. As always, an independent controller is in charge of suppressing the tremor in each joint.

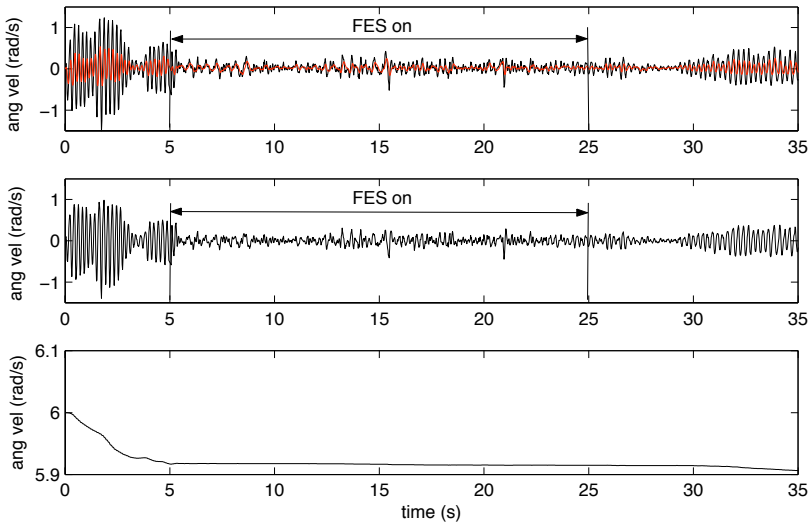

Figure 33. An example of tremor attenuation with the first version of the active strategy. The example corresponds to a patient suffering from Parkinson's disease executing an arms outstretched exercise. Intervals with and without FES are highlighted. The plots correspond to: Top: total wrist movement (black) and voluntary component (red), Middle: tremor component, and Bottom: estimation of tremor frequency. Analysis was performed online with the two-stage algorithm described in deliverable D4.1

3.2.2. Experimental evaluation

The experiments to validate this strategy were carried out as a part of the same protocol reviewed in subsection 2.2; as a matter of fact trials with the active, semi-active and no stimulation were randomized as explained above. Fig. 33 shows a representative trial of a patient in whom considerable attenuation was achieved. In this case tremor was immediately attenuated when stimulation was set, and reappeared approximately 5 s after the stimulation stopped. Tremor attenuation was consistent, and in average ~ 75 % if we look at its amplitude. We concluded that the active strategy constitutes a feasible alternative for tremor attenuation with FES, as already described in the literature.

3.3. Second version of the active strategy

3.3.1. Strategy overview

As for the second version of the semi-active strategy, this new implementation of the active strategy implements closed-loop modulation of stimulation intensity. The stimulation amplitude is controlled as a function of the tremor intensity at the targeted joint. A LUT translates the control action into stimulation parameters; a calibration phase is carried out when the system is set for identification of such table. The controller is also a proportional controller which gain is manually selected based on the relationship between the amplitude of the movement elicited and

the stimulation amplitude applied to the antagonist muscles. Next we describe in more detail the strategy; notice that several aspects are taken from the second version of the semi-active strategy.

Fig. 34 shows a block diagram of the second version of the active strategy for one degree of freedom. The controller comprises a simple repetitive control loop [57] that imposes a "zero tremor" reference to the user's joint (left). The reason for implementing a repetitive controller is that we want to execute a given command many times (attenuate the tremor), and that the system is returned to the same initial condition on the desired trajectory (that in our case is no tremor) [58]. Repetitive control theory has been specially applied to rejection of periodic disturbances [59-61] hence it seems a natural alternative here.

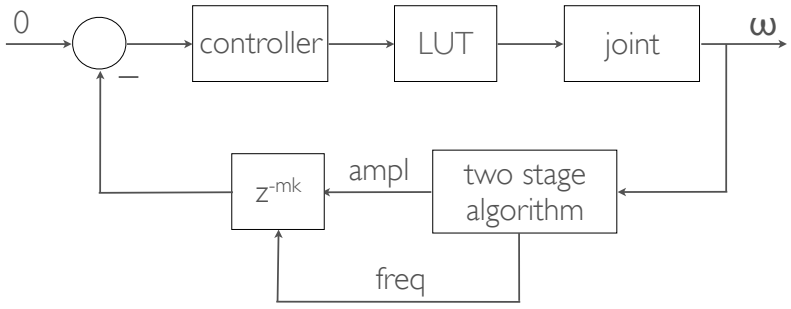

Figure 34. Block diagram of the second version of the active strategy. This controller is implemented for each targeted degree of freedom (or anatomical joint in our case).

Basically, the controller decomposes the joint rotation into concomitant voluntary and tremulous movements using the algorithm described in subsection 2.3. This algorithm also estimates the frequency and intensity of the tremor, which in turn serve to generate the control action for the next tremor period. The control action for a tremor period is therefore scheduled at its beginning based on the previous one; thus the controller can be considered to implement a learning mechanism [58]. This version implements a simple proportional controller which output depends solely on the intensity of the tremor during the last period. The phase of the stimulation is also derived from the tremor estimation by zero cross detection.

As for the semi-active strategy, the controller can be triggered when tremor onset is detected from any sensor modality; at the current model our cognitive Human-Robot Interface detects tremor onset both from inertial sensors and surface EMG (see deliverable D4.1).

The only conceptual difference with respect to the second version of the semi-active strategy is how the stimulation is delivered; i.e. the temporal patterns of stimulation. The decomposition of the total movement in voluntary movement and tremor, the estimation of tremor frequency and amplitude, the calculation of the control output follow the same scheme that for such version of the semi-active strategy. Also do the detection of tremor onset and the initialization of the WFLC. Therefore, next we will focus on the control of temporal patterns of stimulation.

The temporal pattern of stimulation is defined by two variables: the frequency the alternating pattern has to track, which corresponds to the tremor frequency, and the phase of the tremor, since the goal is to artificially elicit an oscillation that is exactly in counter-phase with respect to it. As mentioned above, we use again the WFLC estimation of tremor frequency (24), and the phase is adjusted based on the zero cross of the tremor estimate, since it corresponds to a change from extension to flexion or vice-versa, and hence immediately indicates that the muscle to be stimulated needs to be switched. Moreover, this serves to compensate for errors in tracking tremor frequency in the presence of unexpected events, such as abrupt twitches induced by stimulation (although these happen very rarely). This approach is doable since the online estimation has inherent no delay [38].

Finally, we also applied the same criterion that for the corresponding version of the semi-active strategy to update the control action: if the frequency prediction has an error of more than 20 ms the controller output is not adjusted. Again, this criterion is restarted if the error lasts more than 10 real tremor periods.

3.3.2. Experimental evaluation

This strategy was evaluated in the same experimental session that the second version of the semi-active strategy, see subsection 2.3. Briefly, the experimental protocol comprised two phases i) the calibration of stimulation parameters of the user, and ii) the tremor suppression experiments.

The calibration of the active strategy consisted in the elicitation of alternating movements with different amplitudes and a frequency close to that of the user. A LUT that related stimulation amplitude for the pair of

antagonist muscles to the obtained angular velocity was built, typically containing 5 values. In order to minimize the influence of the tremor on the obtained motion, the experimenter looked for the limb pose that minimized its intensity.

Controller parameters were fixed to the same values that for the second version of the semi-active strategy.

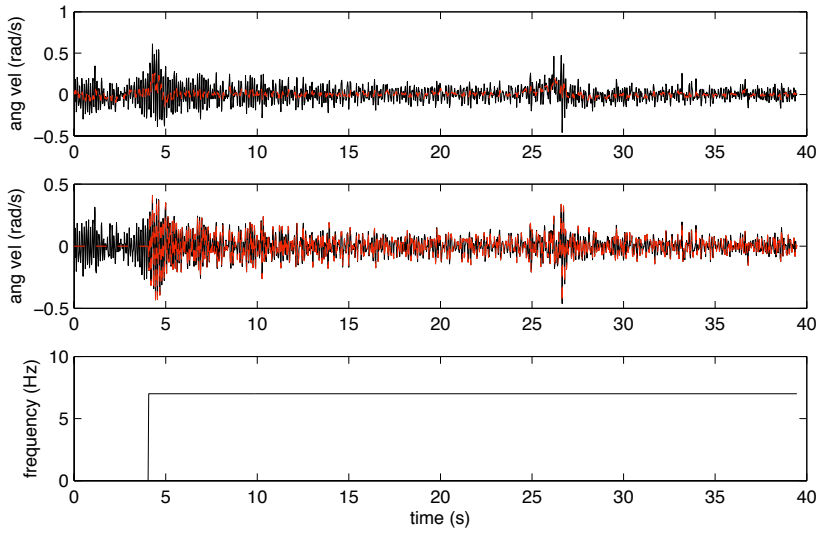

Figure 35. Estimation of tremor amplitude and frequency by the controller implemented in the second version of the active strategy. The example corresponds to an essential tremor patient performing a finger-to-finger test. Top: raw wrist rotation (black) and estimation of volitional component (red); Middle: tremor obtained off-line for comparison sake (black) and online tremor estimation (red) –this estimation is used to extract severity; Bottom: online estimation of tremor frequency.

Here we show an example of tremor suppression with this implementation of the active strategy. The example corresponds to an essential tremor patient performing a finger-to-finger test in order to active his tremor. First Fig. 35 shows the online estimation of voluntary movement and tremor, and the tracking of tremor features, namely amplitude (middle plot) and frequency (bottom plot).

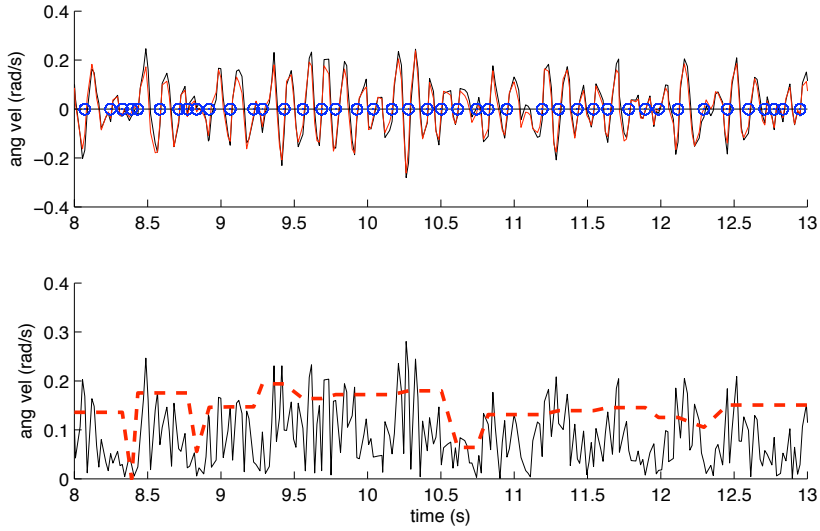

Figure 36. Estimation of tremor amplitude and real frequency (zero-crosses) by the controller implemented in the second version of the active strategy. The example corresponds to an essential tremor patient performing a finger-to-finger test (same as Fig. 35). Top: wrist rotation (black), tremor estimated online (red) and zero crosses obtained online (blue circles); Bottom: rectified wrist motion (black) and controller output (red dashed line).

Next, Fig. 36 shows the instants at which there is a zero cross of the tremor component of movement, and the control action. Zero crosses are employed to switch the stimulation pattern, since it indicates which of the antagonist muscles to stimulate in order to generate the out of phase waveform. We observe that the controller output is not updated when there is a discrepancy (defined to be larger than 20 ms) between the real and

estimated tremor frequency, e.g. at *time* ~ 8.7 s when the tremor is completely attenuated. The controller, however restarts current modulation when they match again. Up to this step, the active strategy follows exactly the same steps that the corresponding version of the semi-active strategy.

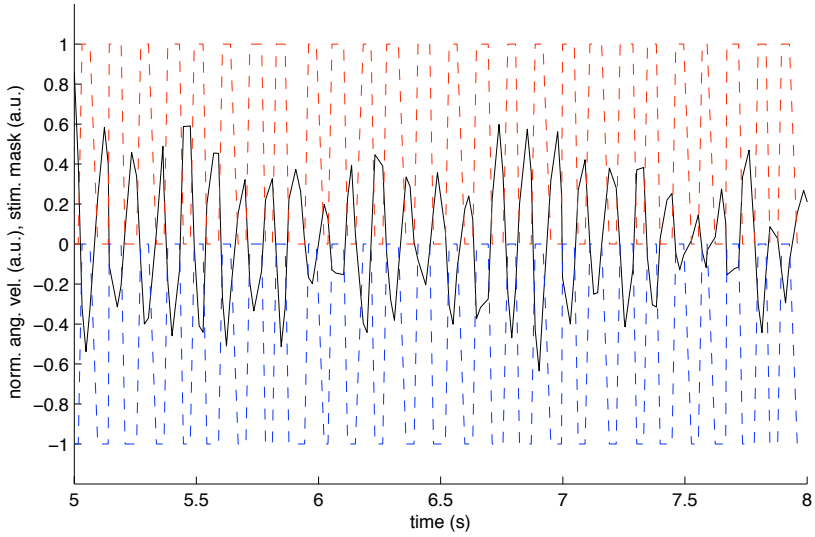

Figure 37. Selection of temporal pattern of stimulation by the controller implemented in the second version of the active strategy. The example corresponds to an essential tremor patient performing a finger-to-finger test (same as Fig. 35). The figure shows the online estimation of tremor (black), and a binary signal that indicates that the wrist extensors (red) or flexors (blue) are to be stimulated. The sign convention for the stimulation corresponds to that of the angular movement.

Fig. 37 shows the temporal pattern of stimulation. Such pattern is obtained based on the frequency estimation provided by the WFLC and the simple phase estimation derived from the zero crosses of the tremor estimation. Notice that the latter is employed to correct the former. Since the algorithm to estimate tremor features has no delay, accurate selection of the muscle to be stimulated (temporal pattern) is achieved. This example shows that tremor frequency is not altered by the stimulation as reported in the literature [13].

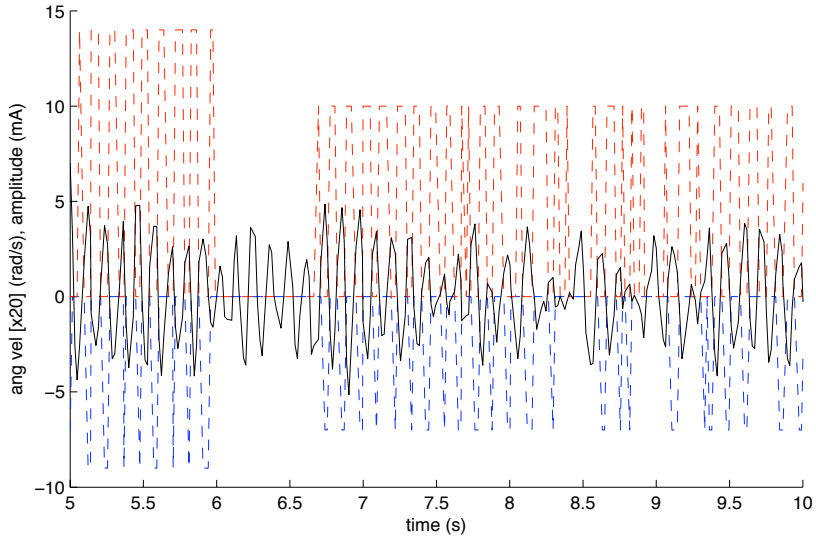

Figure 39. Attenuation of tremor with the second version of the semi-active strategy. The example corresponds to an essential tremor patient performing a finger-to-finger (same as Fig. 35). The plot shows the online estimation of tremor (black) and the stimulation patterns for wrist extensors (red) and flexors (blue). Tremor amplitude is scaled [x 20] for visualization sake.

Finally, Fig. 38 shows the resultant stimulation pattern after conversion of the controller output with the LUT identified during calibration. This can be formulated as the convolution of the temporal pattern of stimulation shows in the previous figure, and the control action represented in Fig.36. Stimulation is turned off at *time* ~6 s

because zero stimulation amplitude was defined for a targeted angular velocity below 0.12, which is the case. Afterwards the tremor appears again (amplitudes in the range of 0.10 are attributed to sensor noise) and hence the controller starts the stimulation again.

3.4. Third version of the active strategy

3.4.1. Strategy overview

This section describes the implementation of the last version of the active strategy. As for the case of the last version of the semi-active strategy, the major changes it implements with respect to second version (of the active strategy) are: i) independent control of muscles acting on a joint, ii) replacement of the LUT by a transfer function that consists in a linear function with saturation, and iii) inclusion of an integral term into the controller. Justification on these modifications is given in subsection 2.4, a block diagram that summarizes the control strategy is shown in Fig. 40.

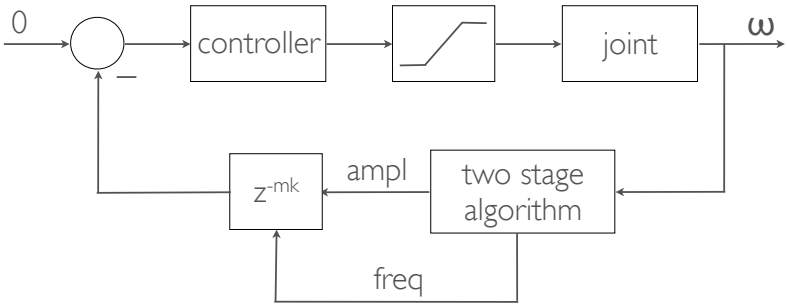

Figure 40. Block diagram of the third version of the semi-active strategy. This controller is implemented for each targeted muscle; therefore two independent controllers drive each anatomical joint.

The implementation is as follows. Joint rotation is as always decomposed into concomitant voluntary and tremulous components. Estimation of tremor frequency is employed to define the period of the next control action, which will be modulated by the intensity of the tremor. A proportional-integral controller which output is translated to a stimulation command by means of a linear transfer function with saturation is used. The saturation represents the maximum output the controller might apply, and is defined as the stimulation parameters that generate a large amplitude oscillation. If the system reaches to the user's tolerance limit this value will define the saturation point.

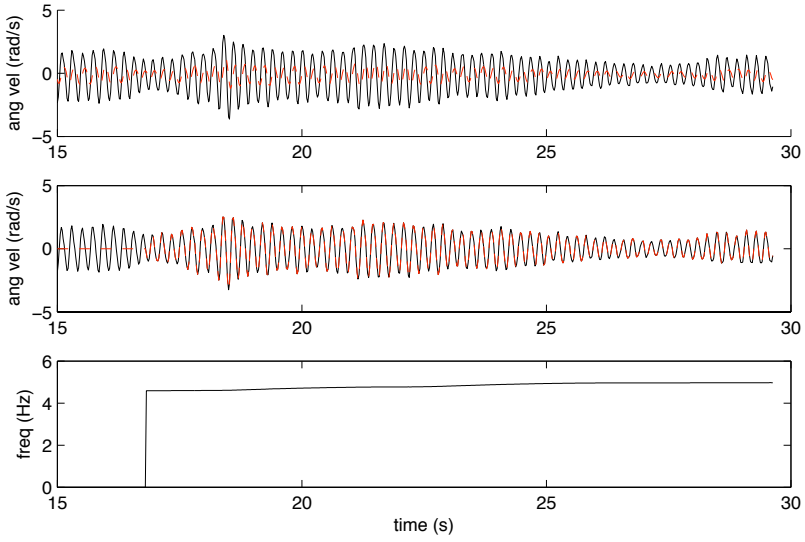

Figure 41. Estimation of tremor amplitude and frequency by the controller implemented in the third version of the active strategy. The example corresponds to an essential tremor patient performing a postural task. Top: raw wrist rotation (black) and estimation of volitional component (red); Middle: tremor obtained off-line for comparison sake (black) and online tremor estimation (red) –this estimation is used to extract severity; Bottom: online estimation of tremor frequency.

This strategy integrates all the modifications implemented in the third version of the semi-active strategy into the second version of the active strategy. Therefore, the decomposition of joint rotation, the detection of tremor onset, the estimation of tremor parameters and the generation of the control action are immediately taken from what is

described in subsection 2.4. The phase of the stimulation pattern is derived from the tremor estimate; zero crosses are employed both to switch the muscle to be activated (i.e. to define the phase of the tremor and ensure out of phase stimulation) and to correct the estimation of tremor frequency.

3.4.2. Experimental evaluation

Once more this strategy was evaluated with patients in the same session that the corresponding version of the semi-active strategy; the reader is referred to subsection 2.4 for details on the protocol. As always the protocol was split into: i) calibration of the system on the user and ii) the tremor suppression experiments.

The calibration of the active strategy in this case consisted in finding the saturation of the controller. We proceeded as follows: as always we looked for the maximum amplitude during independent muscle activation, and then, starting from this value, we increased the stimulation amplitude in order to generate an oscillation with an amplitude considered by the experimenter to be maximal, typically over that of the tremor. Conditions (e.g. limb pose, postural or rest conditions) that minimized the tremor were chosen.

Controller parameters are the same that in subsection 2.4.

Finally we describe a representative example of the third version of the control strategy in an essential tremor patient performing a postural task that consisted in keeping both arms outstretched, and maintain this position against gravity. First, Fig. 41 shows the decomposition of wrist movement into its volitional and tremulous components and the frequency estimation that, as always, shows small variation during an exercise.

Next, Fig 42 shows the online detection of a zero cross of the tremor component, which is employed to select the temporal pattern of stimulation since it indicates a change in the sense of rotation. As expected from the intrinsic non-zero phase of the algorithm, no delay is observed, a feature that is critical for the adequate performance of the active strategy. The lower plot represents the control action to be applied to each muscle, subtle asymmetries in the tremor are observed (e.g. at *time* ~ 18.3 s). These asymmetries also justify the use of independent controllers per muscle, since the required actuation will not be symmetric either.

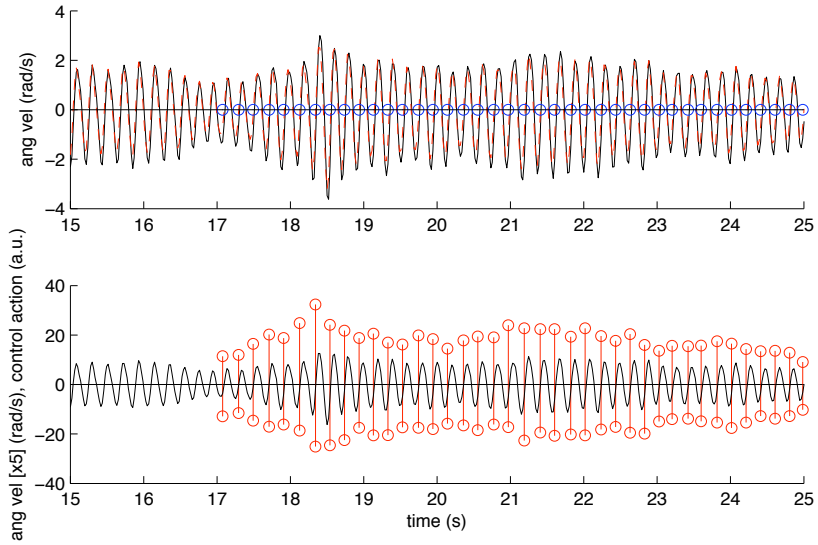

Figure 42. Estimation of tremor amplitude and real frequency (zero crosses) by the controller implemented in the third version of the active strategy. The example corresponds to an essential tremor patient performing a postural task (same as Fig. 41). Top: wrist rotation (black), tremor estimated online (red) and zero crosses obtained online (blue); Bottom: tremor estimated online (black) and control output per period (red). A wrist extension is represented as positive; the control output follows the same convention.

Fig. 43 shows the proportional and integral components of the control action for both the wrist extensors and flexors. As expected the proportional term of the controller reproduces the waveform of the tremor (inverted because the control action for the flexors is generated as a function, of wrist extension and vice-versa), and the integral term continues adding since the system does not manage to suppress completely the tremor. This continuous integration does not pose any practical inconvenience in terms of modulation of stimulation since the saturation term in the transfer function at the output of the controller compensates for it.

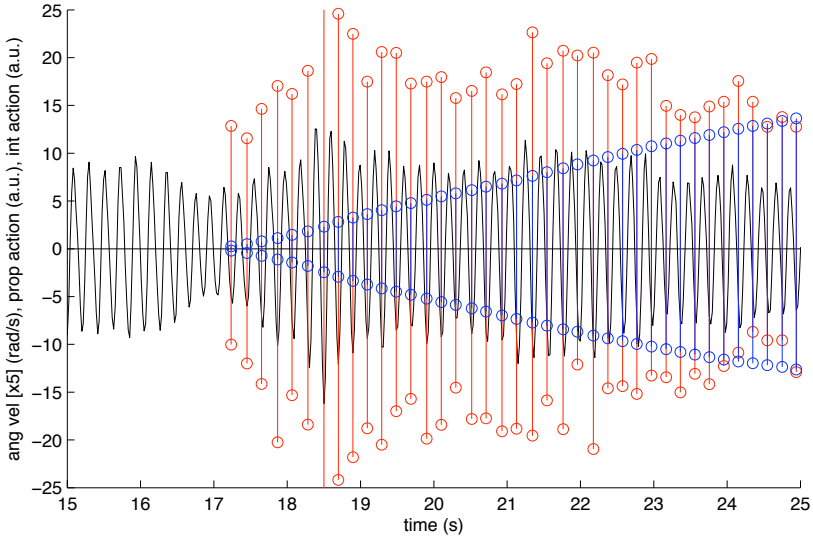

Figure 43. Proportional and integral terms for the controllers of wrist extensors and flexors with the third version of the active strategy. The example corresponds to an essential tremor patient performing a postural task (same as Fig. 41). The plot shows the online estimation of tremor (black) and the proportional (red) and integral (blue) components of the control action. The control actions are represented when they are first applied. A positive action is applied to wrist extensors, a negative to wrist flexors. Each discrete value represents a tremor period, when the controller is updated. Tremor amplitude and the integral term are scaled [x 5] for visualization sake.

Fig. 44 shows the translation of the controller output to stimulation parameters. As explained in the previous subsection, the net output is defined by the convolution of the output of the controller and the temporal patterns of stimulation obtained as explained for the second version of the strategy (an example is shown in Fig S). Although the controller manages to attenuate the tremor (the $R_{spectral}$ defined below equals 0.736; see section 4), it rapidly saturates because of the considerably high residual tremor. This might be due to the fact that the saturation threshold for this patient was defined as a very low level.

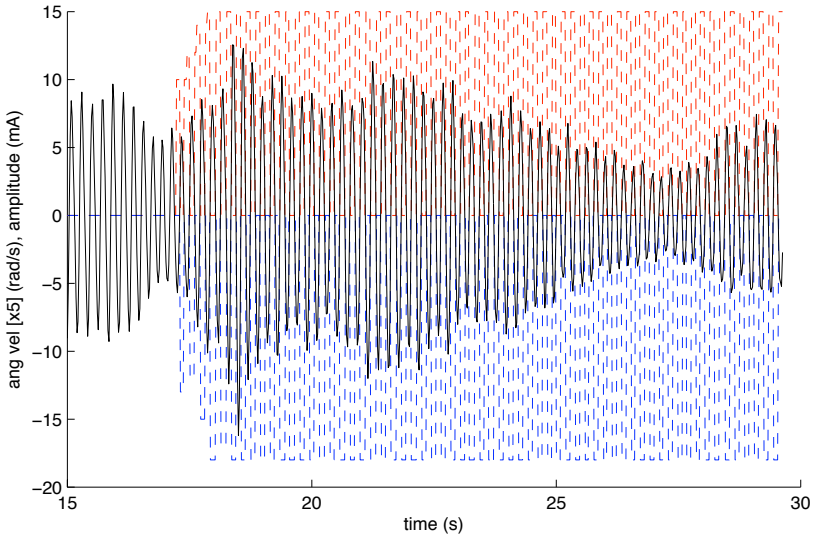

Figure 44. Attenuation of tremor with the third version of the active strategy. The example corresponds to an essential tremor patient performing a postural task (same as Fig. 41). The plot shows the online tremor estimation (black) and the stimulation patterns for wrist extensors (red) and flexors (blue). Tremor amplitude is scaled [x 5].

3.5. Alternative version of the active strategy

Results obtained from the experimental evaluation of the active strategy presented so far (i.e. inertial sensor driven) were highly variable, which was explained by the fact that considerable differences in muscle activation patterns exist for different types of tremor. As a matter of fact, it has been recently suggested that at rest,

tremorogenic muscles of Parkinson's disease patients are activated in counter-phase whereas in essential tremor patients the activation bursts appear synchronized [62]. Our experiments are in agreement with such conclusion. Notice that this aspect was not important when directly acting on the joint with external actuators [11].

Therefore, the Consortium decided to evaluate an EMG-driven version of the active strategy. The concept, which is illustrated in Fig. 45(a) is similar to that of the active strategy: an adaptive filter [63] estimates tremor frequency from the rectified surface EMG signals and provides with the temporal patterns of stimulation. A fixed stimulation intensity (that follows a sinusoidal pattern, see Fig. 45(b)) is then applied to muscles. Periodically, stimulation is blanked in order to update the temporal pattern of stimulation, since the artifacts induced by the stimulation hamper precise EMG processing. A slight overlapping of stimulation patterns (co-contraction) is employed to compensate for the electromechanical delay; this concept will be included in the future implementation of the inertial sensor-driven active strategy, since it seems to improve stability.

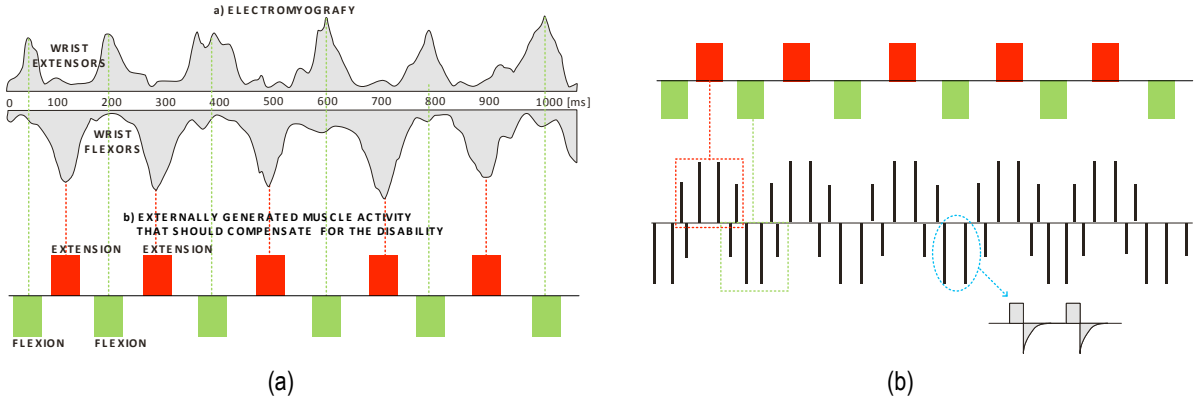

(a) (b)

Figure 45. Alternative version of the active strategy, driven by surface EMG. (a) Concept; (b) Stimulation profiles.

In conclusion, we have developed an active tremor suppression strategy that attenuates the tremor by stimulating the antagonist muscles out of phase, which corresponds to an adaptive notch filter at tremor frequency. The controller is again not model-based but instead relies on instantaneous tremor features to drive the stimulation. As for the IMU driven strategy, individual muscle control and the implementation of a proportional-integral algorithm seem to provide enough adaptation to the physiological variability that underlies neurostimulation. Inclusion of a model in a model-based adaptive impedance controller is identified as future work. Regarding the EMG driven strategy, preliminary tests indicate that the direct inclusion of surface EMG in the control loop might improve the performance of the system since it provides with a more detailed description of muscle activation.

4. Figures of merit to quantify tremor suppression

This section summarizes work on task WP6.4 “”Definition of figures of merit.” This task aims at developing figures of merit to compare the different control strategies developed in tasks WP6.2 and WP6.3, and to complement the clinical and usability metrics defined in work packages WP1 and WP8. The reader is referred to deliverable D8.2 for a detailed description of them.

CSIC led this task and collaborated with IBV on the definition and evaluation of the metrics. It must be mentioned here that 4 aspects were to be considered in these metrics according to the DoW: i) selectiveness, ii) ability to provide zero phase suppression, iii) preservation of voluntary movement, and iv) efficiency versus computational cost. As for the first and third aspect, we believe the best way to address this is to ask the patient to perform the same task with a certain control strategy and without stimulation. This was done during the usability trials performed in work package WP8, and which results are included in deliverable D8.2. Regarding the second item, zero-phase is ensured by the signal cHRI itself [38], therefore we do not consider it in the proposed figures of merit. With respect to the fourth item of the list, all strategies can be run on a simple one-core laptop running QNX Neutrino, and no significant difference on computational load is observed among them. Therefore metrics presented here focus solely on quantification of tremor suppression.

Experimental sessions were exploited to discuss our metrics and elaborate on that. As a matter of fact the observations in the previous paragraph raised after algorithm development, programming and data analysis. Our workflow followed the next items:

- Evaluation of an initial figure of merit based on simple spectral analysis.
- Analysis of experimental data based on such metric.
- Consideration of the aspects highlighted at the beginning of the project (described at the beginning of this section).
- Development and evaluation of a novel figure of merit.

The first figure of merit consisted in a simple ratio between the power of the tremor when the system is in suppression mode and when it is in monitoring mode; i.e. when the system applies FES or not. Such ratio is defined in (30). This figure of merit was employed to evaluate similar systems in the literature, e.g. [11, 13].

$$R = \frac{P_{suppresion}}{P_{monitorization}} \tag{30}$$

were $P_{suppression}$ represents the peak of the power spectrum during tremor suppression (which corresponds to tremor frequency unless the tremor is completely cancelled), and $P_{monitorization}$ the peak of the power spectrum during monitorization.

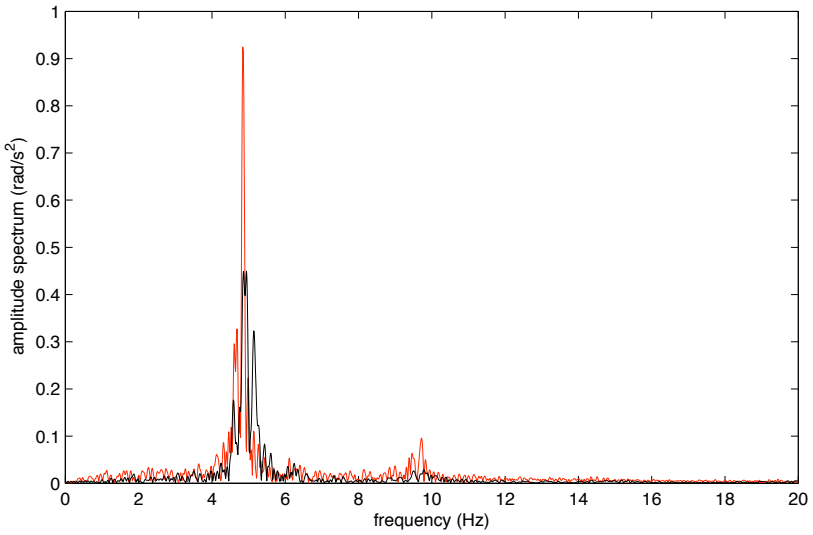

Figure 46. Comparison of amplitude spectra during tremor monitorization and suppression. This trial corresponds to an essential tremor patient performing a finger-to-finger test (the same that in Fig. V). The red trace corresponds to the amplitude spectrum during the whole monitorization window; the black trace to the suppression window.

Our first approach was to compare trials with stimulation and trials without stimulation. However, we soon observed that variability among trials was very high for some patients, and thus this might lead to misinterpretation of our data. This issue is not surprising since tremor is accepted to be a very fluctuating phenomenon.

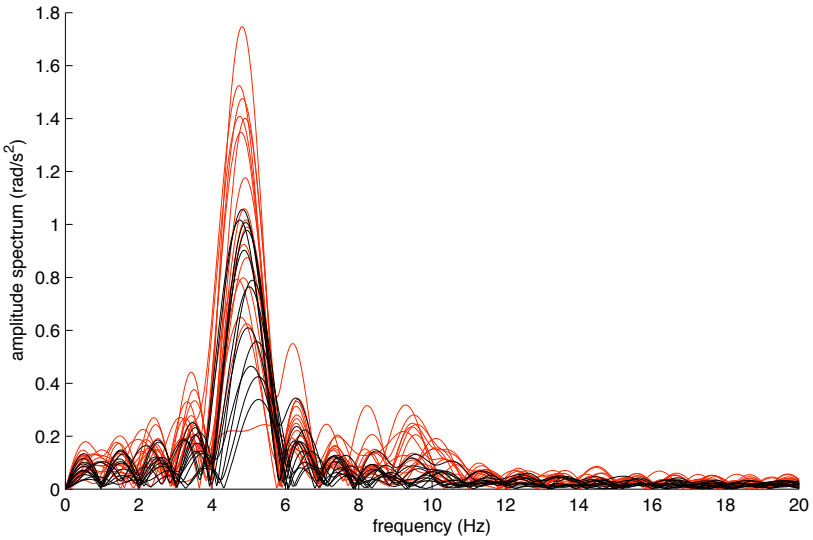

Figure 47. Comparison of amplitude spectra during tremor monitorization and suppression. This trial corresponds to an essential tremor patient performing a finger-to-finger test (the same that in Fig. V). The red traces correspond to the amplitude spectra during monitorization; the black traces to suppression. 1 s disjoint windows are considered in both cases.

Therefore, we decided to define the experimental protocols in such a manner that they alternated a part of the trial without FES and with FES. Normally this was done following the next sequence: no stimulation -stimulation (- no stimulation). But we also concluded that in some cases, also due to the variability of the tremor if we analysed together a window of several seconds we could be misinterpreting the results too. For example, the amplitude spectrum shown in Fig. 46 corresponds to the trial that illustrates the third version of the active strategy which results in terms of tremor attenuation are average; i.e. tremor is not completely attenuated but the results are tangible. If we compare the time window when no stimulation is delivered and the window with the system working we would get the amplitude spectra shown in Fig. 46, and the resultant attenuation obtained from (30) would be R = 0.487. Nevertheless, careful inspection of Fig. V, which shows the whole 30 s trial shows that tremor fluctuates both during stimulation and during its absence. Hence, we decide to split the monitorization and suppression intervals in 1 s, non-overlapping windows. Notice that 1 s windows are a standard the facto in tremor analysis (see e.g. [64]). The resultant amplitude spectra are shown in Fig. 47; considerable variation in between windows of the same condition (stimulation or no stimulation) is observed.

Then for comparison sake we decided to compare the median of the peak of the spectra in both conditions:

$$R_{spectral} = \frac{\tilde{P}_{suppresion}}{\tilde{P}_{monitorization}} \tag{31}$$

were $\tilde{P}_{suppresion}$ represents the median of the peaks of the spectra during suppression, and $\tilde{P}_{monitorization}$ the median of the peaks of the spectra during monitorization.

We decide to use the median instead of the mean due to the well-known sensibility of the later to extreme scores in small populations (we normally have populations of 15 peak powers in each condition). To complement the analysis we also represented the first and third quartiles and the outliers, should there be any; an example of this analysis is shown in Fig. 48. For the case here illustrated the attenuation according to (31) is $R_{spectral}$ = 0.736, which is very different to the value derived from the figure of merit first considered (R = 0.487). We consider, however that the latter provides a more realistic representation of the performance of a certain strategy since it accounts more precisely for tremor fluctuations both in the presence and absence of FES.

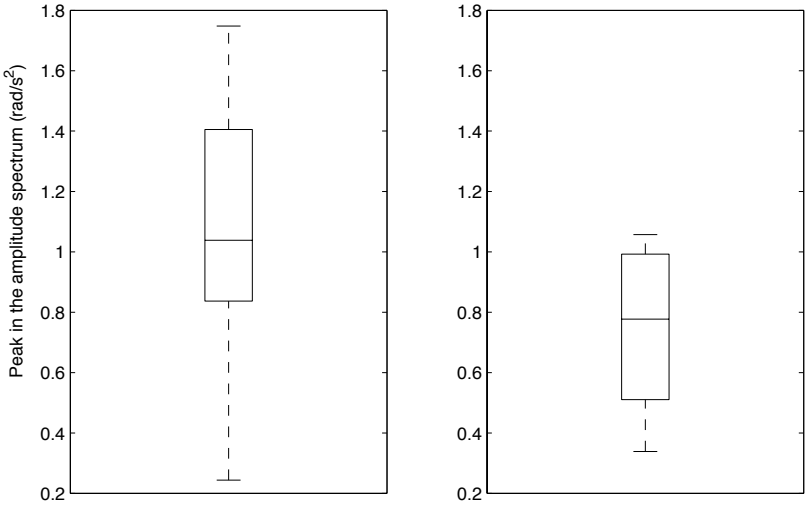

Figure 48. Boxplot that compares the peaks of the amplitude spectra in monitorization (left) and suppression modes (right). The central mark in the box represents the median, the edges of the box the 25th and 75th percentiles; the whiskers extend to the most extreme data points not considered outliers.

In conclusion, we have proposed a figure of merit that serves to compare tremor suppression strategies, and that could be employed to compare any tremor therapy. Its contribution when compared to approaches already presented in the literature is the fact that it accounts for the inherent non-stationarity of the tremor and of its management.

6. Conclusions

This deliverable has described the Consortium effort to develop and evaluate tremor suppression strategies relying on FES. As foreseen in the DoW, two different concepts have been explored, the so-called active and semi-active strategies. The former relies on the generation of an out-of-phase oscillation that counteracts the tremor acting like a notch filter at tremor frequency, whereas the latter is based on the modification of limb impedance in order to cancel the tremor without impeding the concomitant voluntary movement; this is possible because tremor has larger frequency that volitional motions. In this regard, in the current document we detail the implementation and evaluation of a number of versions of both strategies, together with our preliminary tests to evaluate their feasibility. Moreover, we implemented a preliminary version of a surface EMG driven version of the active strategy given that it could improve the inertial-sensor based, since activation patterns are largely different among tremor groups, and very important for this approach.

Apart from this, we have developed a series of tools to enhance the performance of tremor suppression strategies, and permit their evaluation. As for the evaluation of tremor suppression strategies we have developed a novel figure of merit that estimates tremor cancellation accounting for its inherent non-stationarity. We have also implemented a simple communication protocol that achieves full controllability of the TREMUNA stimulators, allowing for flexible validation of our strategies. On the other hand, the Consortium has come up with a simulation model that gives some insights into the importance of electrode geometry in this kind of applications and, on the basis of this, implemented a protocol for automatic definition of electrode shape once the user wears the system. Finally, we have also proposed an easy-to-identify joint model.

According to what has been above presented, we consider milestones M6.1 “Models for muscle stimulation,” M6.2A “Preliminary semi-active tremor control strategy,” M6.2B “Semi-active tremor suppression control strategy,” M6.3A “Preliminary active tremor control strategy,” M6.3B “Active tremor suppression control strategy” and M6.4 “Control strategies for tremor suppression” to be met. No additional task related to this work package is active.

References

[1] Rocon E, Belda-Lois JM, Sánchez-Lacuesta JM and Pons JL. Pathological tremor management: Modeling, compensatory technology and evaluation, *Tech Disab* 16: 3-18, 2004.

[2] Joyce GC and Rack PMH. The effects of load and force on tremor at the normal human elbow joint, *J Physiol* 240: 375-396, 1974.

[3] Elble RJ. Physiologic and essential tremor, *Neurol* 36: 225-231, 1986.

[4] Héroux ME, Pari G and Norman KE. The effect of inertial loading on wrist postural tremor in essential tremor, *Clin Neurophysiol* 120(5): 1020-1029, 2009.

[5] Kotovsky J and Rosen MJ. A wearable tremor suppression orthosis, *J Rehab Res Develop* 35: 373-387, 1998.

[6] Michelis J. Introducing the Neater-Eater, *Action Res* 6: 2-3, 1988.

[7] Adelstein BD. Peripheral mechanical loading and the mechanism of abnormal intention tremor, MSc Thesis, 1981.

[8] Pons JL (editor), Wearable robots: Biomechatronic exoskeletons, John Wiley & Sons, 2008.

[9] Hendriks J, Rosen MJ and Huang S. A second-generation joystick for people disable by tremor, *Proc RESNA Conf* 1991.

[10] Rosen MJ, Arnold AS, Baiges IJ, Aisen ML and Eglowstein SR. Design of a controlled-energy-dissipation orthosis (CEDO) for functional suppression of intention tremors, *J Rehab Res Develop* 32: 1-16, 1995.

[11] Rocon E, Belda-Lois JM, Ruiz AF, Manto M, Moreno JC and Pons JL. Design and validation of a rehabilitation robotic exoskeleton for tremor assessment and suppression, *IEEE Trans Neural Syst Rehab Eng* 17(3): 367-378, 2007.

[12] Prochazka A, Elek J and Javidan M. Attenuation of pathological tremors by functional electrical stimulation: I Method, *Ann Bioemd Eng* 20(2): 205-224, 1992.

[13] Javidan M, Elek J and Prochazka A. Attenuation of pathological tremors by functional electrical stimulation: II Clinical evaluation, *Ann Bioemd Eng* 20(2): 225-236, 1992.

[14] Bó APL and Poignet P. Tremor attenuation using FES-based joint stiffness control, *Proc 2010 IEEE/RAS Int Conf Robot Automat*.

[15] Widjaja F, Shee CY, Au WL, Poignet P and Ang WT. Using electromechanical delay for real-time anti-phase tremor attenuation system using Functional Electrical Stimulation, *Proc 2011 IEEE/RAS Int Conf Robot Automat*.

[16] Manto M, Rocon E, Pons JL, Belda-Lois JM and Camut S. Evaluation of a wearable orthosis and an associated algorithm for tremor suppression, associated algorithm for tremor suppression, *Physiol Meas* 28(4): 415-425, 2007.

[17] McNeal DR. Analysis of a model for excitation of myelinated nerve, *IEEE Trans Biomed Eng* 23(4): 329-337, 1976.

[18] Coburn B. A theoretical study of epidural electrical stimulation of the spinal cord–part ii: Effects on long myelinated fibers, *IEEE Trans Biomed Eng* 32(11): 978-986, 1985.

[19] Hodgkin AL and Huxley AF. A quantitative description of membrane current and its application to conduction and excitation in nerve, *J Physiol* 117(4): 500-544, 1952.

[20] Sweeney JD, Mortimer JT, and Durand D. Modeling of mammalian myelinated nerve for functional neuromuscular stimulation, *Conf Proc IEEE Eng Med Biol Soc* 1577-1578, 1987.

[21] Rattay F. Electrical nerve stimulation theory, experiments and applications, Springer, Wien, 1990.

[22] McIntyre CC, Richardson AG, and Grill WM. Modeling the excitability of mammalian nerve fibers: influence of afterpotentials on the recovery cycle, *J Neurophysiol* 87(2): 995-1006, 2002.

[23] Rattay F. Modeling the excitation of fibers under surface electrodes, *IEEE Trans Biomed Eng*, 35(3): 199-202, 1988.

[24] McIntyre CC and Grill WM. Extracellular stimulation of central neurons: influence of stimulus waveform and frequency on neuronal output, *J Neurophysiol* 88(4):1592-1604, 2002.

[25] Reichel M, Martinek J, Mayr W, and Rattay F. Functional electrical stimulation of denervated skeletal muscle fibers in 3d human thigh - modeling and simulation, *Proc Int Vien Work Func Elect Stim*, 44-47, 2004.

[26] Martinek J, Reichel M, Rattay F, and Mayr W. Analysis of calculated electrical activation of denervated muscle fibres in the human thigh, *Proc Int Vien Work Func Elect Stim* 228-231, 2004.

[27] Lertmanorat Z, Gustafson KJ, and Durand DM. Electrode array for reversing the recruitment order of peripheral nerve stimulation: experimental studies, *Ann Biomed Eng*, 34(1):152-160, 2006.

[28] Kuhn A, Keller T, Lawrence M and Morari M. A model for transcutaneous current stimulation: simulations and experiments, *Med Biol Eng Comput* 47(3): 279-289, 2009.

[29] Kuhn A, Keller T, Micera S and Moraria M. Array electrode design for transcutaneous electrical stimulation: A simulation study, *Med Eng Physics* 31(8): 945-951, 2009.

[30] Kuhn A and Keller T. A 3D transient model for transcutaneous functional electrical stimulation, *Int Funct Electr Stim Soc Conf* 10: 385-387, 2005.

[31] Prodanov D and Feirabend HK. Morphometric analysis of the fiber populations of the rat sciatic nerve, its spinal roots, and its major branches, *J Comp Neurol* 503: 85-100, 2007.

[32] Sha N, Kenney LPJ, Heller BW, Barker AT, Howard D and. Wang W. The effect of the impedance of a thin hydrogel electrode on sensation during functional electrical stimulation, *Med Eng Phys* 30(6): 739-746, 2008.

[33] Bijelic G, Popovic-Bijelic A, Jorgovanovic N, Bojanic D and Popovic D. E Actitrode: The new stimulation interface for functional movements in hemiplegic patients, *Serbian J Electr Eng* 1(3): 21-28, 2004.

[34] Fujii T, Seki K and Handa Y. Development of a new FES system with trained Super-Multichannel Surface electrodes", *Int Funct Electr Stim Soc Conf* 2004.

[35] Popovic-Bijelic A, Bijelic G, Jorgovanovic N, Bojanic D, Popovic M and Popovic DB. Multi-Field surface electrode for selective electrical stimulation, *Artif Organ* 29(6): 448-452, 2005.

[36] Popovic DB and Popovic M. Automatic determination of the optimal shape of a surface electrode: Selective stimulation, *J Neurosci Meth* 178: 174-181, 2009.

[37] Rocon E, Andrade AO, Pons JL, Kyberd P and Nasuto SJ. Empirical mode decomposition: A novel technique for the study of tremor time seris, *Med Biol Eng Comput* 44: 569-582, 2006.

[38] Gallego JA, Rocon E, Roa JO, Moreno JC and Pons JL. Real-time estimation of pathological tremor paramters from gyroscope data, *Sensors* 10: 2129-2149, 2010.

[39] Riener R and Quintern J. A physiologically based model of muscle activation verified by electrical stimulation, *Bioelectrochem Bioenerg* 43(2): 257-264, 1997

[40] Riener R and Fuhr T. Patient-driven control of FES-supported standing up: A simulation study, *IEEE Trans Rehab Eng* 6(2): 113-124, 1998.

[41] Ferrarin M, Palazzo F, Riener R and Quintern J. Model-based control of FES-induced single joint movements, *IEEE Trans Neural Syst Rehab Eng* 9(3): 245-257, 2001.

[42] Page A, Candelas P and Belmar. On the use of local fitting techniques for the analysis of physical dynamic systems, *Europ J Phys* 27(2): 273-279, 2006.

[43] De Leva P. Adjustments to the Zatsiorsky-Seluyanov's segment inertia parameters, *J Biomech* 29(9): 1223-1230, 1996.

[44] Rocon E, Ruiz AF and Pons JL: Biomechanical modelling of the upper limb for orthotic tremor suppression, *Appl Bionic Biomech* 2(2): 81-85, 2005.

[45] Hogan N. Adaptive control of mechanical impedance by coactivation of antagonist muscles, *IEEE Trans Autom Control* 29(8): 681-690, 1984.

[46] Burdet E, Osu R, Franklin DW, Milner TE and Kawato M. The central nervous system stabilizes unstable dynamics by learning optimal impedance, *Nature* 414: 446-449, 2001.

[47] Riley PO and Rosen MJ. Evaluating manual control devices for those with tremor disability, *J Rehabil Res Dev* 24: 99-110, 1987.

[48] Deuschl G, Raethjen J, Lindemann M and Krack P. The pathophygiology of tremors, *Muscle Nerve* 24(6): 716-735, 2001.

[49] Mann KA, Werner FW and Palmer AK. Frequency analysis of wrist motion for activities of daily living, *J Orthop Res* 7: 304-306, 1989.

[50] Brookner E. Tracking and Kalman filtering made easy, John Wiley & Sons, Hoboken, NJ (USA), 1998.

[51] Riviere CN, Rader RS and Thakor NV. Adaptive cancelling of physiological tremor for improved precision in microsurgery, *IEEE Trans Biomed Eng* 45: 839-846, 1998.

[52] Widrow B, Glover JR, McCool JM *et al*. Adaptive noise cancelling: Principles and applications, *Proc IEEE* 63: 1692-1716, 1975.

[53] Hellwig B, Häussler S, Schelter B *et al*. Tremor correlated cortical activity in essential tremor, *Lancet* 357: 519-523, 2001.

[54] O'Suilleabhain PEO and Matsumoto JY. Time-frequency analysis of tremors, *Brain* 121: 2127-2134, 1998.

[55] Widjaja F, Shee CY, Poignet P and Ang WT. FES artifact suppression for rea-time tremor compensation, *Conf Proc IEEE Int Conf Rehab Robot* 2009.

[56] Widjaja F, Shee CY, Poignet P and Ang WT. Filtering of intended motion for real-time tremor compensation in human upper limb using surface electromyography, *Conf Proc IEEE Eng Med Biol Soc* 2009.

[57] Hara S, Yamamoto Y, Omata T and Nakano M. Repetitive control system: A new type servo system for periodic exogenous signals, *IEEE Trans Autom Control* 33(7): 659-668, 1988.

[58] Longman RW. Iterative learning control and repetitive control for engineering practice, *Int J Control* 73(10): 930-954, 2000.

[59] Tomizuka M, Tsao TC and Chew KK. Analysis and synthesis of discrete-time repetitive controllers, *J Dynam Syst Meas Control* 111: 353-358, 1989.

[60] Steinbuch M. Repetitive control for systems with uncertain period-time, *Automatica* 38(12): 2103-2109, 2002.

[61] Chew KK and Tomizuka M. Digital control of repetitive errors in disk drive systems, *IEEE Control Syst Mag* 10(1): 16-20, 1990.

[62] Nisticó R, Pirridano D, Salsone M *et al*. Synchronous pattern distinguishes resting tremor associated with essential tremor from rest tremor of Parkinson's disease, *Parkinsonism Related Disord* 17(1): 30-33, 2011.

[63] Popovic LZ, Sckara TB and Popovic MB. Adaptive band-pass filter for tremor extraction from inertial sensor data, *Comp Meth Program Biomed Eng* 9: 298-305, 2010.

[64] Halliday DM, Conway BA, Farmer SF, Shahani U, Russell AJC and Rosenberg JR. Coherence between low-frequency activation of the motor cortex and tremor patients with essential tremor, *Lancet* 355: 1149-1153, 2000.

Appendix. Definition of commands for the FES hardware

Here we describe activities on task WP6.5 "Definition of strategies for rule-based control of the multi-channel FES hardware." This task aims at defining the control interface for the FES hardware developed in the framework of the project.

AAU led this task and collaborated with CSIC and UNA in the different activities. A number of research visits and telemeetings devoted to hardware integration, design specifications, coordination and testing were carried out. The final outcome of such activities was a novel multichannel programmable stimulator described in deliverable D3.3, and a multi-platform communication protocol. Here we describe the current implementation in the TREMOR platform, which is based on QNX Neutrino (see deliverable D7.1 for details).

The work on this task has been carried out as follows:

- Preliminary tests with simple control strategies and using a commercial not fully controllable stimulator provided by UNA Systems.
- Analysis of the outcome of these tests and preparation of design specifications at conceptual, hardware and software levels.
- Implementation of a communication protocol in QNX Neutrino.
- Definition of control rules that are incorporated in the strategies presented in sections 2 and 3.

Communication protocol for TREMUNA stimulators

Here we summarize the communication protocol that we have developed for the control of TREMUNA stimulators. Briefly, each stimulator is implemented as an object of the class `cFES`. Methods to change single or groups of parameters in a single channel and/or multiple channels are available. The protocol is easy to use and flexible, and has been employed for the implementation of all the strategies presented in this document.

Object or Method		Purpose
`channel`	`Channels[8]`	Object that contains all parameters of the 8 channels of the stimulator.
`bool`	`Mode`	Object that informs whether the stimulator is on or off.
`handle`	`USBport`	Object that assigns a USB port to the stimulator.
`unsigned char`	`Mask`	Object that defines what stimulator channels are active.
`cFES(int USB)`		Constructor of a stimulator object.
`void`	`STARTON()`	Method to turn the stimulator on.
`void`	`SHUTDOWN()`	Method to turn the stimulator off.
`void`	`SETMASK()`	Method to change the mask (active channels) of the stimulator.
`void`	`SetCurrent(int ch2s)`	Method to change the current intensity delivered by each channel.
`void`	`SetFreq(int ch2s)`	Method to change the frequency of the stimulation pulses delivered by each channel.
`void`	`SetPW(int ch2s)`	Method to change the pulse width of the stimulation pulses delievered by each channel.
`void`	`SetPN(int ch2s)`	Method to set the number of pulses that each channel delivers.
`void`	`setDT(int ch2s)`	Method to send an activation delay to the stimulator.
`void`	`SetParameters()`	Methods that sends all parameters to all the stimulator channels

Table VI. Methods and objects of the cFES class, which implements the control interface for the stimulators.